UNIVERSITY OF
BIRMINGHAM

The Application of Genetic Algorithms to Parameter Estimation in Lead-Acid Battery Equivalent Circuit Models

Thesis submitted in accordance with the requirements of
the University of Birmingham for the degree of
Master of Philosophy

in

School of Electronic Electrical & Computer Engineering

by

Shen Guo

May 2010

to my parents

Acknowledgements

First and foremost, I would like to express my sincere appreciation to my supervisors, Dr. Stuart Hillmansen and Dr. Jihong Wang, for their support, guidance, inspiration and patience during my MPhil study. I have greatly benefited from their knowledge and experience.

I am also grateful to Dr. Jianlin Wei and Dr. Nan Jia for their support and advices during my research and to Dr. Leonid Shpanin for his assistance in my laboratory experiments. Many thanks to Mr. Bo Fan, Mr. Shaofeng Lu and Mr. Lei Chen for their valuable ideas shared with me. I would also like to thank Mr. Hao Sun, Mr. Xing Luo as well as all the other colleagues for their discussions and their kind assistant during my study.

Finally, I would like to thank my family and all my friends. Without their encouragement, support and understanding, this thesis would not have been possible.

Abstract

Batteries are becoming increasingly important to our life as they are applied in a range of different areas. Therefore the reliability of battery is a critical issue in these battery applications. It has been noticed that most batteries have limited cycle durability, that is, the total capacity drops when a battery is charged and discharged for a number of cycles. If a battery is too weak to offer sufficient energy, it should be replaced at the right time. But current problem is that there is no reliable method available to quantify the capacity loss and to estimate whether the remaining capacity of battery. Complete discharge, which is the only way of capacity estimation, has a negative effect to the battery plates therefore it cannot be used too frequently.

This thesis summarises the research work in the development of the battery status estimation algorithm. The work initially focused on the mathematical descriptions of lead acid batteries, and a mathematical model based on this study was then developed and implemented to describe the process of battery discharge. Genetic Algorithms (GAs) were used as a tool to identify the parameters related to the battery, including the internal resistances, state of charge, and capacity. The relevant simulation results show that the model is able to adequately simulate the battery discharge process.

The aforementioned models were extended to a further investigation of the batteries state of health. It was noticed that there is a link between the status of

battery health and the internal resistance. In this project, six batteries were discharged and charged in several times in order to simulate the capacity loss that occurs in normal operation. This capacity loss is related to the state of health, and the parameter estimation was able to adequately distinguish between different state of health.

These results indicate that the internal resistance increases when the state of health of a lead-acid battery decreases. This progress is at first very slow when the battery is new but the change becomes faster when the remaining capacity of battery drops to about 75% of the initial. It is found in the thesis that the value of internal resistance is increased by 25% approximately when the state of health is brought down to about 50%, meaning that the battery cannot offer enough energy as new and should be replaced for safety consideration.

The method described within this thesis performed adequately in the limited tests performed during the experimental work. Further investigations are recommended in order to refine the method which is potentially suitable for online implementation in battery condition monitoring systems.

Contents

List of Figures

Chapter 1
Background and Objectives of the Project

1.1. Overview

Fossil fuels have been the main energy resource in recent human history, although their continuing use has been shown to have a detrimental effect on the environment. The principal problem for fossil fuels is that they cannot be reproduced within a short period of time, so it is a finite energy supply source. If current consumption rate continues, they will be exhausted in a few generations from now. Fossil fuel has never been considered as a clean-resource because there is an emission of noxious gasses including CO CO_2 NO_x SO_x and HC into the atmosphere. With all the pressure from the problems associated with the fossil fuel, exploration of the usage of renewable energy is becoming an increasingly important issue.

Wind energy, hydro energy, and solar energy are three of the most important renewable energy sources and they have been implemented on a large scale: wind energy has produced a annual global total of 650.19×10^{12} W·h (74,223 MW×24h×365 days) (Anon 2006) energy in the year 2006, and hydro

energy is about 3.04×10^{15} W·h (3040.4×10^{12} W·h) (Anon 2007). Solar energy resources are estimated at about 1069.4×10^{15} W·h (3850×10^{21} J) (Smil 2007), To compare with the worldwide energy consumption of 130.97×10^{15} W·h in the year 2007, it is clear that renewable energies have a significant role to play (Anon 2007).

However, the problem of the implementation of the renewable energy is that the electricity generated is intermittent and the power systems are experiencing the problem of rapidly changing power demand. Therefore the management of the energy is an important issue. Devices of energy storage should solve these problems in theory.

1.2. Review of Energy Storage Systems

Not only giving a large scale energy solution, energy storage devices are also commonly used in a range of applications related to everybody. Different energy storage technologies are suited to different applications and consideration must be made in order to select the correct solution for each application. This section will give an overview of the existing energy storage systems.

1.2.1. Applications of the Energy Storage Systems

Large scale energy storage systems, which are also called grid energy storage, refer to the methods used to large-scale store electricity within an electrical power grid. Off-peak energy is stored during times when production (from power plants)

exceeds consumption and the stores are utilized at times when consumption exceeds production. In this way, electricity production need not be drastically scaled up and down to meet momentary consumption – instead, production is maintained at a more constant level.

Despite the applications in grid scale, the energy storage systems are also popular in a number of areas. For example they are usually used to optimize the energy generated from the engine in modern electrical hybrid vehicles. One such application is in a shunter locomotive. A shunter is a small railroad locomotive intended for assembling trains ready for a road locomotive to take over, disassembling a train that has been brought in, and switching a train to another rail at the rail terminals. The duty cycle of a shunter is characterised by short duration high power demands (accelerating a rake of vehicles) and the long periods of idling while the train waits for other operations. Comparing to traditional shunter locomotive that use diesel engines only for the whole duty cycle, hybrid shunter locomotives with energy storage devices can have a 40-70% reduction in fuel use (RailPower Hybrid Technologies n.d.). This saving is made by operating the prime mover at its optimum.

Another application of energy storage in the vehicle technologies is the regenerative braking system, which is used to save the braking energy of vehicle. The potential of this technology to save energy for a vehicle is depends on the duty cycle (Lu, Meegahawatte et al. 2008), which is characterized by storing the energy generated when the vehicle is decelerating and releasing when accelerating.

Energy storage devices are also very popular in stationary applications, also known as the Uninterruptible Power Supply (UPS) systems. This system is designed to meet the power demand when problems like power failure happen and it is important especially in the applications where power failures could have serious consequences, for example, in hospitals and computer centres (Berndt 2009).

The energy storage devices in the UPS system are often used to achieve "uninterruptible" in a short period before the secondary power supply started. When a power problem occurs, the energy storage device starts to supply electricity immediately, and at the same time, the generator begins to start. When the generator is ready to supply sufficient power the energy storage device stops providing power. When the grid power is recovered, the energy storage device can be recharged until full.

1.2.2. Review of the Existing Energy Storage Devices

There are various kinds of energy storage systems, including pumped hydro, compressed air, flywheel, supercapacitors, electrochemical, and also superconducting magnetic. Each technology is suited to different applications and careful consideration must be made in order to select the correct solution for each application.

Pumped hydro is the oldest and the most effective kind of large scale energy storage method, which have been used for nearly a century since 1929 (Juvonen

2003). Two large reservoirs at different altitudes, with a pump, a turbine, a motor and a generator are employed to collect the off-peak energy. The water is released from the higher one through a turbine to generate electricity during peak load period.

Compressed air is a pneumatic energy storage method that refers to the air kept under a certain pressure. This system can be used in grid energy storage that the air can be stored by compressors during periods with low power demand. This compressed air can be released to a generator to meet the high power demand during peak time (Glendenning 1981; Ter-Gazarian 1994; Juvonen 2003). In some applications, the compressed air is released through a combustor mixed with natural gas to obtain a higher overall efficiency.

A capacitor is an electrical device that can store energy in an electric field between a pair of conductors and is often used in circuits for short term energy storage. It blocks the circuit to hold DC voltage. Supercapacitors are energy storage devices with the same principle, but with a higher energy density. The power density of the supercapacitor systems can be very high, but the energy is often released in a very short duration (Ter-Gazarian 1994). As a result the supercapacitors are usually used in applications of an energy burst.

Superconducting magnetic energy storage system stores energy in the magnetic field generated by direct current in a coil. Instead of traditional wires like copper, superconductors are employed to avoid the energy consumptions as heat because of the resistance. A problem is that the optimal operating temperature for

superconductors is 50-77K, a refrigerator is therefore necessary in the system for cooling down.

Flywheels are considered as a method of storing mechanical kinetic energy by accelerating a flywheel to a very high speed to store the energy, and decelerating to release the energy. Flywheels are very efficient for short duration storage cycles due to their fast response speed. These energy storage devices are used mainly in applications that demand kinetic energy storage, and high numbers of deep discharge cycles.

Electrochemical energy storage stands for the device capable of converting chemical and electrical energy to each other by chemical reactions. Batteries are the most common technology of electrochemical energy storage methods. The oxidation and reduction reactions in the two electrodes of battery lead to the current through the external circuit when discharging to provide energy. The secondary battery can be recharged by applying electrical current, which reverses the chemical reactions that occur during the discharge.

Fuel cell is another technology with very high energy density that converts the chemical energy in a source fuel into an electrical current. The fuel cells are considered as the “environmental friendly” as the only by-product is water. The working principle of fuel cells when discharging is the same as the batteries, but unlike the batteries, the fuel cells do not need recharge as they only provide electrical energy while the active chemicals are supplied to the electrodes (Mantell 1984; MPowerSolutionsLtd. n.d.).

Figure 1-shows the Ragone chart of the energy and power density of some energy storage systems.

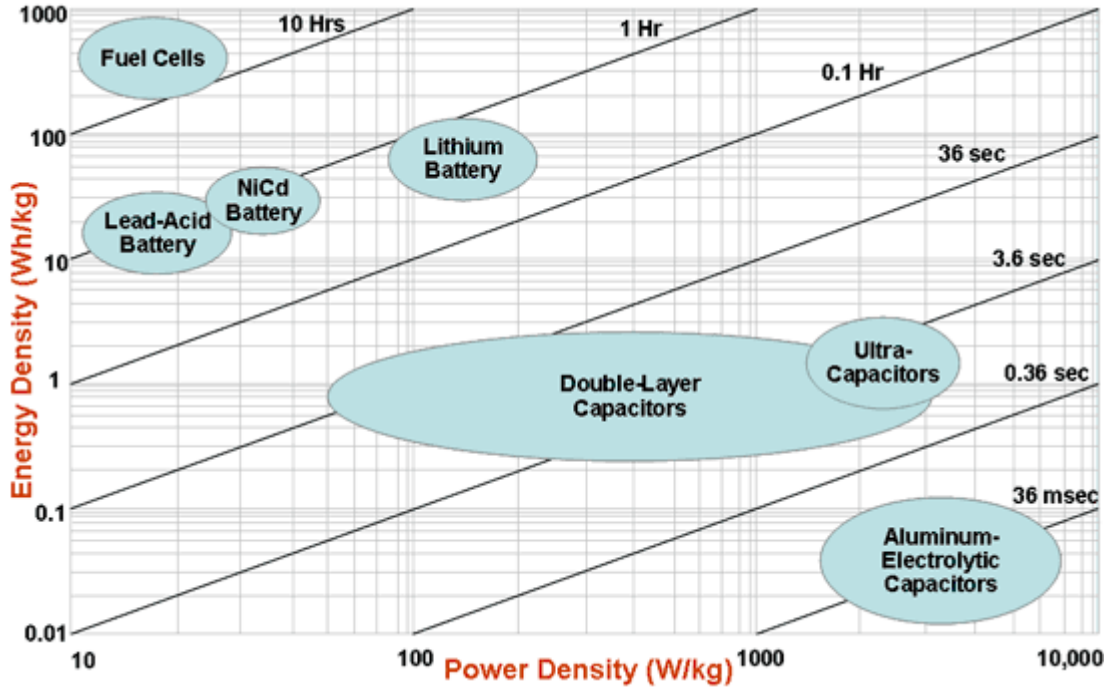

Figure 1-1 Power density vs. energy density plot (MPowerSolutionsLtd. n.d.)

1.2.3. Review of Batteries

The preceding discussion has identified that energy storage devices are becoming increasingly important in both stationary and mobile applications. Battery, as the most popular energy storage device, is studied in this section.

There are two different types of batteries applied in a large range of areas now: Primary batteries and Rechargeable batteries. Primary batteries, which are also called disposable batteries, often have higher energy densities than the rechargeable ones, and they have a lower self-discharge (Ter-Gazarian 1994).

However, as the chemical reactions in these batteries are not reversible and the active materials cannot be restored to their initial forms, these batteries cannot be reliably recharged. The primary batteries are intended to be used once and then discarded, therefore they are not suitable for the energy storage systems.

Rechargeable battery is the other type of the electrochemical batteries, which is also known as secondary battery because their electrochemical reactions are electrically reversible. There are many different rechargeable battery technologies, in which only four of them are leading the world market: nickel-cadmium, nickel-hydride, lead-acid and lithium-ion (Berndt 1993; Berndt 2009).

The Nickel-cadmium (NiCd) battery is a kind of rechargeable battery that uses nickel oxide hydroxide and metallic cadmium as electrodes, and an alkaline electrolyte (often potassium hydroxide) (Mantell 1984). As designed to compete the primary batteries, the NiCd batteries are often manufactured in the same size and they are used in the consumer market as primary batteries, for example in clocks, toys, radios and cordless tools. However, when the NiCds are substituted for primary cells, the lower terminal voltage and smaller ampere-hour capacity may reduce performance as compared to primary cells. The most attractive feature of the nickel-cadmium batteries is that they are more difficult to damage comparing with other batteries during deep discharge cycles. They can also sustain more cycles, and the lower internal resistance can also help achieve a higher maximum discharge rate. A problem preventing the large scale application of this battery technology is that the nickel-cadmium batteries suffers faster self discharge rate than other rechargeable batteries, and the cadmium used as the

active material in one of the electrodes is toxic and expensive (Zhang, Liu et al. 2010). Furthermore, the capacity loss caused by the continuously discharge and recharge to the same state of charge, called “memory effect”, is also a very important issue of the nickel-cadmium batteries (Sato, Takeuchi et al. 2001).

The nickel-metal hydride (NiMH) battery is a type of secondary electrochemical battery that designed to substitute for the nickel-cadmium cells. They have a similar size and a similar cell voltage but with more advantages. By using hydrogen-absorbing alloy as negative electrode instead of cadmium, this electrochemical technology is considered as “environmental friendly” because of the absence of toxic cadmium (Berndt 1993). The nickel-metal hydride batteries also have low internal resistance and the high cycle durability as the NiCds, and a NiMH battery can have two to three times the capacity of an equivalent size nickel-cadmium battery. However, the nickel-metal hydride batteries also have a similar high self-discharge rate as the nickel-cadmium batteries (Lee, Lee et al. 1996), and it also cannot afford complete discharges. Memory effect from repeated partial discharge can occur in a NiMH battery, but this is reversible through charge cycling (Berndt 2009).

The lead-acid batteries are the oldest type of rechargeable battery with a history of over 150 years, but they are still the most popular battery chemistry for applications such as engine starting or backup power systems, as there is no cheaper alternative when weight is not a factor. This technology uses lead and lead dioxide as electrodes and an acid electrolyte of sulphuric acid and the advantage of this configuration is that the electrolyte takes part in reactions of

both electrodes, and both electrodes turn into lead sulphate when discharging (Berndt 1993; Berndt 2009). The lead-acid batteries can be designed for not only deep discharge cycles but high discharge rate, or compromise of the two cycles. They have a lower self-discharge rate compared with the nickel batteries, and they also do not suffer from the memory effect (Mantell 1984; Berndt 2009). However, as the energy density of lead-acid battery is not high, it is seldom applied in the portable electronics. Another important problem is that the lead-acid batteries must be recycled as the active material "lead" is toxic to both the environment and the human bodies (Bernardes, Espinosa et al. 2004).

The lithium-ion (Li-ion) batteries are almost the perfect cell chemistry and are currently used a wide range of consumer electronics products including cameras, cell phones, laptops, etc. They have many attractive performance advantages which make them also ideal for higher power applications such as automotive and standby power. First of all, the lithium-ion batteries have the highest energy density in all the rechargeable battery now, which is about 4 times better than lead-acid (Jacobi 2009). They are also capable for deep discharge and high discharge rate, with a relatively slow self discharge. There is no liquid electrolyte in the lithium-ion batteries, which means they are immune from leaking. However, just opposite to the lead-acid batteries, the most serious problem that discourages the lithium-ion batteries is the low economic efficiency comparing with the lead-acid batteries. Other factors like the stability of the chemicals and the recycling of lithium should also be concerned because of the chemical activeness of lithium.

Table 1-1 is gives some basic properties of the four major rechargeable batteries

introduced above. There are also some less common battery chemistries used by rechargeable batteries in addition to these technologies, including nickel-zinc (NiZn), nickel-iron (NiFe), etc, but they have a small market share. For the four major battery chemistries, lead-acid batteries, with their low price and high flexibility, is adopted in a wide range of application areas.

Table 1-1 properties of the rechargeable batteries (Wikipedia n.d.)

Type	Voltage (V)	Energy Density (Wh/kg)	Power Density (W/kg)	Self Discharge rate	Cycle Durability
Nickel-Cadmium	1.2	40-60	150	20%	1500
Nickel-Metal-Hydride	1.2	30-80	250-1000	20%	1000
Lead-Acid	2.1	30-40	180	3%-4%	500-800
Lithium-ion	3.6	160	1800	5%-10%	1000-1200

1.2.4. The Management of Batteries

In the areas that batteries are employed as the energy storage device, it is a critical issue to consider that whether there is enough energy in the battery to meet the demand. However, batteries do have the problem in limited cycle durability, that is, when a battery is charged and discharged for a number of cycles, its total capacity decreases. If the battery cannot offer sufficient power/energy, it should be replaced at the right time. But the problem is that it is difficult to quantify the capacity loss and when the capacity of battery is no longer sufficient for a particular application. Due to the limitation of batteries, it is essential to develop a method to determine the capacity of battery that subjected to various duty cycles in a number of applications.

1.3. Project Objectives

The main objective of the project is to develop a method which can determine the key parameters of batteries from the discharge tests. The proposed methodology is a model based approach, that is, to develop a mathematical model of the battery which can represent the dynamic performance and battery status and characteristics can be investigated through the analysis of the model.

The first step of the project is to build a mathematical model of battery. The dynamic model is expected to reflect the relevant behaviours of battery when being discharged including the characteristics of State of Charge, Depth of Charge, Electromotive force, Terminal Voltage. The unknown parameters in the model are identified by using Genetic Algorithms (GAs) with the laboratory experimental data. Afterwards, some batteries are tested in experiments and the parameters in different state of health are recorded to analyze the battery in different status of battery.

The focus of this work is to develop a suitable method for parameter identification for common battery systems. The lead-acid battery has been chosen because it has relatively well defined properties and there is a wealth of literature describing the performance of these types of batteries. From an experimental view point they are also readily available of low cost.

1.4. Outline of the thesis

The thesis is organized into seven chapters and the first chapter presents the background and motivation of the research project. The remaining chapters are briefly described as follows:

Chapter 2 gives an overview of lead-acid batteries including the development, working principle and also some modern battery designs and technologies. In the second part of chapter 2, important concepts for a battery, including electromotive force, capacity, state of charge, internal resistance and state of health, are introduced and some mathematical descriptions of these concepts are discussed.

Chapter 3 starts from some requirements of the mathematical model designed for this project, and several different methods of battery model approaches are discussed. Afterwards some details of the dynamic mathematical model are analyzed. The initial battery model is described in the last part of this chapter that summarized the equations of the battery.

Chapter 4 is mainly focused on some improvement of the mathematical model described in chapter 3. In the first section of chapter 4, the experimental test rig in the project is introduced. Some findings in the experimental tests is then listed and studied and integrated into the improved model. Finally the SIMULINK implementation and a simulation study are given.

Chapter 5 presents a method of model parameter identification. The principle of

Genetic Algorithms is studied at first. Then this algorithm is employed in the model and the parameters of the model are identified with the help of experimental tests. This chapter also includes the validation of battery model using two other groups of test results.

Chapter 6 develops an algorithm that can reflect the state of health of a lead-acid battery. In this chapter, the internal resistance parameters are measured under different state of health through a group of continuous experimental tests. The change of internal resistance under a specific working condition is then related to the battery state of health.

Finally, Chapter 7 gives a summary and the conclusions of the project. Also the future works that can be improved are proposed in this chapter.

Chapter 2
Introduction of Lead-acid Batteries

This chapter gives an overview of lead-acid batteries including background knowledge, working principles, explanation of terminologies, technologies, and applications encountered for this technology. The chapter presents the fundamental knowledge and prepares for the project work to be reported in the following chapters.

2.1. A General Overview of the Lead-acid Battery

The lead-acid battery is the oldest type of rechargeable battery. The first example of a lead-acid battery can be attributed to the German physicist Sinsteden who published the performance data of this battery system in 1854 (Berndt 1993). Later in 1859, the French physicist Planté realized that a plate construction was required to achieve a much larger effective surface area, and he produced the first rechargeable battery which was marketed for commercial use by alternately charging and discharging lead sheets, immersed in sulphuric acid. This method has remained unchanged and still in use today in stationary applications (Berndt

1993; Wikipedia n.d.). One of the first applications of lead-acid batteries was for storing electrical energy for telegraphy systems. The capacity required for these applications was low, and the battery at that time was not yet suited to high power industrial applications (TNI_Ltd. 2007).

In 1880, a French chemical engineer Fauré significantly improved the design of the lead-acid battery by producing the active materials separately. His method was to coat the lead plate with a paste of lead oxides, sulphuric acid and water in a warm humid atmosphere. The paste then changed into a mixture of lead sulphates which adhered to the lead plate as an electrochemically active material. As a result of this technology, the Fauré cells are able to achieve much higher capacity with the first charge in comparison with the Planté ones (Berndt 1993; TNI_Ltd. 2007). The problem of these plates is that they are not very durable and become weak only after a few discharge/charge cycles. The lead grid alloyed with antimony or calcium was developed to improve the mechanical characteristics. The holes on the grid are able to achieve improved bonding thus the batteries may have a longer lifetime. This advantage led to the industrial manufacturing of lead-acid batteries. In 1881, a lead electrode with a ribbed surface was designed in order to have a large effective surface of the active material, and this was the pioneer of the large surface plates which are still common today (Berndt 1993; TNI_Ltd. 2007; Wikipedia n.d.).

In the beginning, lead-acid batteries were operated in open jars. The advantage of this feature was that the electrode can be cleaned and exchanged easily, but faced the problem of water evaporation. Therefore the early batteries have to refill water

in order to continue normal use. However, this problem can be dramatically reduced when the cells were fitted with covers to limit the evaporation (Berndt 1993). This kind of battery design is known as a 'flooded lead-acid battery'.

In the 1950s, a new type of battery, which was aimed to become spill-proof, was designed and manufactured on a large scale. This type of battery is characterized by an immobilized electrolyte, however this kind of spill-proof battery was only manufactured in small sizes up to about 10 Ah (Berndt 2001). Later, the combination of a valve improved the characteristic features of the lead-acid battery, and this kind of battery is still common today, and is known as the Gel Lead-acid battery (Berndt 1993). In the 1970s, micron diameter glass fibres, originally designed for air filters, were used in glass mats which absorbed the electrolyte and acted as separator. Soon this kind of Absorbent Glass Mat (AGM) battery appeared in market for stationary application.

Currently, Valve Regulated Lead Acid (VRLA) batteries based on both AGM and Gel electrolytes are available in a large range of capacities for both stationary and mobile power applications, with a range of different designs for each type of application. Arguably, the most important application of lead-acid batteries is for vehicle engine starting. The battery employed in this application, which is called Starting, Lighting and Ignition (SLI) batteries, are designed to deliver bursts of energy, usually in a discharge current as large as several hundred amperes in a very short time. A different type of battery construction can produce batteries capable of deep cycling, which are more suited to slow discharge cycles (Tuck 1991; Anon 2007).

2.2. Configuration of Lead-acid Batteries

This section gives a brief description of the working principles of lead-acid batteries and how the battery can be configured to suit different applications.

2.2.1. Electrochemical Principles

The lead-acid battery comprises two electrodes and the electrolyte. The structure of the lead-acid battery is shown in Figure 2-1, in which one electrode is Cathode and the other is Anode. The active matter in the positive plate is made of lead dioxide (PbO_2) and that in the negative plate is made of lead (Pb), and the electrolyte is sulphuric acid. One electrode can serve either as a Cathode or as an Anode depending on which process the battery is experiencing - charging or discharging. With this structure, a battery could convert electrical energy into chemical energy and back again, which is associated with the process of charging and discharging.

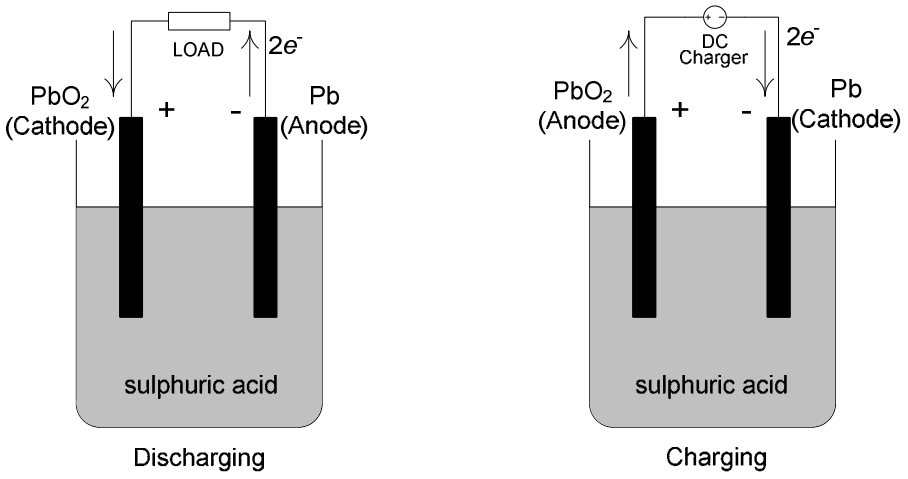

(a) (b)

Figure 2-1 Working Principle of Lead-Acid Batteries, (a) shows the battery when

discharging and (b) is when charging with a DC charger

For the discharging process, as shown in Figure 2-1 (a), the negative plate acts as the anode and the positive plate is the cathode. If a wire is connected between the two, the excess electrons from the anode will travel through the wire as a current to the cathode where they are needed to complete the electron deficient reaction there. The chemical reactions in a lead-acid battery when discharging are described as follow:

Negative plate reaction (Anode):

$$Pb + HSO_4^- - 2e^- \rightarrow PbSO_4 + H^+$$

Positive Plate reaction (Cathode):

$$PbO_2 + HSO_4^- + 3H^+ + 2e^- \rightarrow PbSO_4 + 2H_2O$$

For the charging process, an external power source is connected to the two electrodes with the voltage as shown in Figure 2-1(b). In this way, the flow of electrons is forced backwards, against the electropotential and the reactions are driven backwards, changing the lead sulphate back into lead and lead dioxide on the negative and the positive plates and restoring the sulphuric acid to the liquid electrolyte. The anode when a battery is charging is the positive plate and the cathode is the negative plate and the chemical reactions in a lead-acid battery when charging are described as:

Positive plate reaction (Anode):

$$PbSO_4 + 2H_2O - 2e^- \rightarrow PbO_2 + HSO_4^- + 3H^+$$

Negative plate reaction (Cathode):

$$PbSO_4 + H^+ + 2e^- \rightarrow Pb + HSO_4^-$$

The thermodynamic heat effects caused by the reactions are small in the lead-acid battery, because the difference between the enthalpy and the free enthalpy is very small. The rate of reversible heat effect in the reaction is 13.2 kJ per mol of the cell reaction, which corresponds to about 3.5% of the total energy converted when the lead-acid battery is discharging or charged. This amount of energy is relatively small and is generated over a comparatively long period of time so it is usually easily dissipated through radiation and convection (Berndt 1993).

2.2.2. Lead-Acid Battery Types and Technologies

The flooded battery is the simplest type of lead-acid battery in use. Flooded batteries are common for some traction applications despite the requirement in high maintenance. They are also very common for large capacity backup power supplies for telecommunication, computer centres, grid energy storage, and off-grid household electric power systems. Since the flooded batteries are not sealed, they must be kept upright to avoid acid spills and water must be periodically added to top up the liquid electrolyte. The most attractive feature of the flooded battery is that they are able to withstand certain level of overcharging without damage providing proper maintenance is carried out.

The Valve Regulated Lead-Acid (VRLA) battery, which is often colloquially called the sealed lead-acid battery, is becoming more and more popular in many applications. Because VRLA batteries are mostly sealed, the electrolyte evaporation will be reduced, and spillage can be largely avoided when overcharging, which are very common in flooded batteries. The electrolyte of the

VRLA battery is designed to be immobilized, so the VRLA batteries will not leak if inverted, pierced, or if the container is broken. They can be mounted in any orientation and position even immersed in water. The immobilization of the VRLA electrolyte can be achieved by using an absorbent mat separator as well as gelling materials.

In Absorbent Glass Mat (AGM) battery, the electrolyte is absorbed into a mat of fine glass fibres in order to immobilize the electrolyte. In addition, the pores in the mats are fine enough to prevent the lead dendrites in the cathode from growing through as a separator, and only glass is wetted enough by sulphuric acid can soak the separators. The glass mats can therefore be used to insulate the electrodes.

Gelling is another way to immobilize the electrolyte and this gelling technology at present is only applied for lead-acid batteries. The idea is to mix the sulphuric acid with silica fume (SO_2), which makes the electrolyte gel-like. The mixture is stable over a long term, environmental safe and easy to work technically (Berndt 1993). The sulphuric acid bound by the gel can also insulate electrodes as a separator similarly with that in an AGM battery.

VRLA batteries, including both gel and AGM batteries, are able to recombine and reduce the emission of gases during overcharge, so the requirement for the room ventilation is reduced and there is no acid fume emission during normal discharge (Berndt 1993; Anon 2007; Wikipedia n.d.). Although the generation of hydrogen can be slowed down, it cannot be avoided completely. As a result, a valve regulation safety system is employed in VRLA batteries which vents the gases in

the battery only during over pressure faults (Tuck 1991; Berndt 1993).

However the VRLA batteries do have some drawbacks. First of all, the VRLA batteries tend to have a lower specific energy density than flooded batteries and they are also more expensive. An accurate charging control is very important for a VRLA battery, especially when charging under high temperature environments, since it is not possible to cure the damage caused by overcharge.

2.2.3. Battery Designs for Different Applications

Lead-acid batteries are deployed in a range of applications. Different designs are therefore required due to the different working environments and duty cycles. SLI batteries are designed for a burst of energy for cold-cranking an engine. A SLI battery is supposed to provide power only in the first few seconds when starting an engine, and will be recharged immediately once the engine is started. In this kind of lead-acid batteries, a larger surface area of the electrode plates is used to provide high electric current in a short period. However repeated deep discharge may shorten the battery lifetime.

On the other hand, deep cycle batteries are designed for applications where the batteries are regularly discharged. The plates of the deep cycle batteries are often very thick in order to withstand the frequent and deep discharge cycles. The plate surface area of a deep cycle battery is not as large as a SLI battery, and as a result, it is not possible to offer great power.

Marine batteries are a compromise between a SLI battery and a deep cycle battery. Standby batteries can be classified as marine batteries which are used for backup power supplies and providing the power in emergency situations. They are designed for a long lifetime, and a large capacity, but repeated discharges and high current drain are not the intended application. Traction batteries are designed for higher current drain and repeated, deep discharge cycles. They are usually bigger and heavier than other types of lead acid for the same voltage and capacity, but that is the cost of durability.

2.3. Mathematical Descriptions of Lead-acid Batteries

In order to investigate the relationship between the battery behaviour and remaining lifetime for a lead-acid battery, initial studies have been carried out and are described in this chapter. Concepts including Capacity, State of Charge (SOC), Depth of Charge (DOC), State of Health (SOH), and internal resistance are introduced and quantitative descriptions of these concepts are listed.

2.3.1. Capacity

The capacity of a lead-acid battery represents how much charged energy the battery can offer, which is usually described in Ampere-hours (Ah). The charge capacity of a battery is decided by the construction factors of a battery cell. This includes the materials contained in the electrodes and the acid solution. In addition, the capacity of a battery is not a fixed quantity but varies according to

how quickly it is discharged. This is known as Peukert's law (Ceraolo 2000; Dhameja 2001; Rand, Moseley et al. 2004):

$$C_p = I^k t \tag{2.1}$$

where C_p is the capacity on one-ampere discharge rate, which is a constant

I is the discharge current (A)

t is the time of discharge (h)

k is the Peukert constant and for a lead-acid battery with the value between 1.1 and 1.3 (varies for each individual battery)

It is common to refer to "C_n" as the capacity of battery in Amp-Hours which corresponds to complete discharge of the battery in n hours. "n" is a subscript that represents the discharge rate. In industry, the capacity under ten-hour discharge rate (C_{10}) is always taken as the nominal capacity.

2.3.2. Electromotive force

The electromotive force of a battery cell is the difference between the electric potential of the two electrodes of each cell (Rand, Moseley *et al*. 2004). The potential of each electrode, which is called half cell potential, is decided by the chemical reaction and the relative activities of the solution, and can be obtained from Nernst's equation (Crompton 2000):

$$E = E^0 - \frac{RT}{zF} \ln \frac{\alpha \mathrm{Red}}{\alpha \mathrm{Ox}} \tag{2.2}$$

where E is the half-cell potential (V)

E_0 is the standard half-cell potential (V)

α is the relative activity of the oxidizer (α *Ox*) and reducer (α *Red*)

z is the number of electrons transferred in the cell reaction

R is the universal gas constant which is 8.314472 $J \cdot K^{-1} \cdot mol^{-1}$

T is the absolute temperature

F is the Faraday constant, the number of coulombs per mole of electrons and $F = 9.64853399 \times 10^4$ $C \cdot mol^{-1}$

At room temperature, *RT/F* is a constant of 25.693mV for cells, therefore $\frac{RT}{nF} \ln \frac{\alpha \mathrm{Red}}{\alpha \mathrm{Ox}} = \frac{25.693\mathrm{mV}}{\mathrm{z}} \ln \frac{\alpha \mathrm{Red}}{\alpha \mathrm{Ox}} = \frac{0.0591\mathrm{V}}{\mathrm{z}} \log_{10} \frac{\alpha \mathrm{Red}}{\alpha \mathrm{Ox}}$,

The Nernst's Equation therefore can be expressed by:

$$E = E^0 - \frac{0.0591\mathrm{V}}{z} \log_{10} \frac{\alpha \mathrm{Red}}{\alpha \mathrm{Ox}} \tag{2.3}$$

The electromotive force could be calculated by the difference of the electric potential:

$$EMF = E_{anode} - E_{cathode} \tag{2.4}$$

When a lead-battery is discharging, the electromotive force can be written as:

$$EMF = E^0_{anode} - E^0_{cathode} + \frac{0.0591\text{V}}{z}\log_{10}\frac{\alpha(\text{H}^+)\alpha(\text{SO}_4{}^{2-})}{\alpha^2(\text{H}_2\text{O})} \tag{2.5}$$

The standard half-cell potential of the anode E^0_{anode} is equal to 1.685 (PbO_2-$PbSO_4/SO_4^{2-}$) and that of cathode $E^0_{cathode}$ is -0.356 (Pb-$PbSO_4/SO_4^{2-}$), which are constants for the same battery chemistry. And the number of electrons transferred (n) is 2 for a lead-acid battery.

Therefore, the electromotive force of a lead-acid cell can be obtained by:

$$\begin{aligned} EMF &= 1.685 - (-0.356) + 0.0296\text{V}\log_{10}\frac{\alpha(\text{H}^+)\alpha(\text{SO}_4{}^{2-})}{\alpha^2(\text{H}_2\text{O})} \\ &= 2.041 + 0.0296\text{V}\log_{10}\frac{\alpha(\text{H}^+)\alpha(\text{SO}_4{}^{2-})}{\alpha^2(\text{H}_2\text{O})} \end{aligned} \tag{2.6}$$

This electromotive force of a battery cell is numerically equal to the open circuit voltage, which means that the terminal voltage of a single cell battery when it is disconnected from the external load. For a lead-acid cell, the electrochemical force at fully charged is between 2.10-2.13V per cell.

2.3.3. State of Charge and Depth of Charge

State of charge (SOC) and depth of charge (DOC) are variables that can describe the battery charge. The main difference is that the SOC describes the percentage of remaining charge relative to the nominal capacity while the DOC represents that relative to the actual capacity under a specific discharge current. These two

variables can be obtained by calculating the charge consumed and the battery capacity:

$$SOC = 1 - Q_e / C_{10} \tag{2.7}$$

$$DOC = 1 - Q_e / C_I \tag{2.8}$$

where Q_e is the charge consumed by the load (Ah)

C is the nominal capacity (Ah)

C_I is the actual capacity under the discharge current I (Ah)

2.3.4. Internal Resistance and State of Health

The internal resistance of a lead acid cell is the physical resistance of the cell. The value of the internal resistance is decided by many different factors. But it could be obtained by a simple equation:

$$r = \frac{V_{OC} - V_t}{I} \tag{2.9}$$

where V_{oc} is the open circuit voltage (V)

V_t is the terminal voltage when discharging (V)

I is the discharge current (A)

However the factors in this equation are only a method of calculating the internal resistance but not the determinants. It is shown in applications that the internal resistance of a lead-acid battery will increase when discharging as the SOC and

the DOC drops.

It is common for batteries to suffer a capacity loss when discharged and charged in a number of duty cycles, even when idle. Aged batteries are often weak and sometimes not able to offer enough charges. Therefore they should be replaced or maintained. State of health is a defined variable that is important for a weak battery. This variable is to show how weak the battery is and represents the percentage of remaining capacity to the initial capacity when the battery is brand new (Okoshi, Yamada et al. 2006), as shown in the equation:

$$SOH = \frac{C_{weak}}{C_{new}} \tag{2.10}$$

where C_{weak} is the remaining capacity of a weak battery (Ah)

C_{new} is the capacity when the battery is brand new (Ah).

The reason for the capacity loss is complex, but is usually due to the sulphation. Sulphation is a process when the amorphous lead sulphate, which is easily converted back to lead, lead oxide and sulphuric acid, converts to a stable crystalline form coating the electrodes. This form of lead sulphate cannot conduct electricity and cannot be converted back to lead, lead dioxide and lead sulphate under normal charging conditions. The internal resistance of a lead-acid battery therefore increases and less charge can be provided when discharging. Complete or repeated deep discharges of a battery at low current densities that lead excessive utilization of the active material, are the most critical reason for

capacity loss, for example a discharge of a traction battery that draws more than 80% of its nominal capacity (Berndt 1993).

2.3.5. Multi-Cell Lead-Acid Batteries

In most applications of batteries, the voltage of an individual cell is not enough to provide the sufficient voltage and power supply. The solution is usually to series connect a number of cells in a battery in order to achieve a higher battery voltage. The electromotive force of a series of lead-acid battery cells is directly related to the cell numbers, as well as the charge state of each cell. For a six-cell lead-acid battery, which is a standard for most common usages, the fully charged electromotive force is about 12.8V. The internal resistance of a multi cell battery however, is also equal to the sum of the internal resistances of each cell.

Usually all the cells in a multi-cell battery should be constructed in the same manner and in particular the capacity should be consistent because the capacity of a multi-cell battery will be limited to the cell with the lowest capacity. If one of the cells fails, it is not possible for the current to flow through the cell and the battery is therefore disconnected from its internal cell loss. Also if the SOC of one particular cell drops faster than others in a battery, the electromotive force of that cell may affect the whole behaviour of the battery.

2.4. Summary

The technology development of lead-acid batteries has been continuous over the

last 150 years. From the earliest open cell batteries, different advanced battery configurations are now available, which have been adopted in a wide range of applications. Meanwhile, a number of solutions have been developed to address the battery problems encountered in applications, such as electrolyte evaporation, spillage and the electrolysis of electrolyte when charging. However, there are still issues affecting the efficient and safe use of lead-acid batteries, for example, determination of the SOH, which if addressed in a robust manner would lead to significant improved battery management system performance. This chapter has presented the essential fundamental knowledge, technology terms and working principles of lead-acid batteries, which is served as a preparation for further study reported in the following chapters of the thesis.

In order to reveal the dynamic behaviour of a battery under different SOH and identify the suitable strategy for SOH determination, the mathematical modelling study is carried out and an equivalent circuit model is derived in the next chapter. The key concepts of the battery model are explained and the fundamental analysis is given for the concepts introduced.

Chapter 3
Equivalent Circuit Modelling of Lead-acid Batteries

In order to estimate the status of a battery, a model based approach is adopted in the project. A mathematical model for lead-acid batteries should be developed with a suitable level of abstraction. This chapter describes the requirements to the model to serve the project objectives and reviews the available model technologies. An improved mathematical model for lead-acid batteries is introduced in the late part of this chapter.

3.1. Requirements for the Battery Model

The main objective of the project is to develop an algorithm that can determine the battery health by monitoring the battery status during discharge cycles. This algorithm is designed for implementation in a battery health monitoring system with life-time prediction capabilities. This prediction system is intended to work on applications where the battery performance is of great importance, for instance, hospital UPS systems and vehicle ignition systems. To achieve the objective, the requirements to the mathematical model can be defined as:

Requirement 1: The model should be able to calculate the evolution of key battery parameters, including terminal voltage, cell temperature, the state of health

and the internal resistance, which describe the condition of the battery for dynamical discharging. It should also be able to adequately represent dynamic processes while the battery is discharging.

Requirement 2: The complexity of the model must be sufficient to satisfy the requirement 1, but must also be executable in real-time for a model-based condition monitoring system.

Requirement 3: The output of the battery model should be understandable to the battery operators and technicians as well as meaningful to those who do not have any background in battery technologies.

3.2. Overview of Battery Model Techniques

A number of different types of battery models have been used to serve as a tool in solving a range of problems (GONG 2005). These include Electrochemical Models, Computational Fluid Dynamics Models, Finite Element Models and Equivalent Circuit Models. This section gives an overview to the above named four different types of battery models, and the problems which are addressed by each of them. In Section 3.2.4, every battery model technology is assessed against the overall requirements.

3.2.1. Electrochemical Model

Electrochemistry is a branch of chemistry that studies chemical reactions which

take place in a solution at the interface of an electron conductor (a metal or a semiconductor) and an ionic conductor (the electrolyte). The reactions involve electrons transfering between the electrode and the electrolyte or species in solution. The application of electrochemistry research directly leads to the development of the lead-acid batteries.

Behaviour of a battery depends not only on how the battery is used but also on a number of construction factors (Ruetschi 2004). These factors include but are not limited to: the thickness of the plates, the active mass density of the active material, the concentration of the acid solution, and the geometry of the electrodes (Berndt 2001; Ruetschi 2004)

The electrochemical model is mainly focused on the oxidation/reduction reactions between the electrolytes and the electrodes. By analyzing the consistency of each matter in the solution and the electrochemical reaction caused by the connection of electrodes to external circuit, it is possible to represent the dynamic behaviour of the battery (Crompton 2000).

3.2.2. Physical Models

The finite element method is a numerical analysis technique for finding approximate solutions of partial differential equations as well as of integral equations. The basic principle of the Finite Element Model (FEM) is to divide the problem into elements and each element is a smaller problem to be solved so that they could be analyzed separately. The ‘elements’ are then be assembled together

to restore the initial problem.

Finite element is a very popular method of analysis in those areas with a complex geometry and it is good at stress and thermal analysis. For batteries, the Finite Element Models can help with a good understanding of the heat loss and that for vibration problem in mobile applications. There are also attempts to analyze the current density on the positive grid bar in a lead-acid battery using FEM (Ball, Evans et al. 2002).

Computational Fluid Dynamics (CFD) technology is a well-established tool for physical analysis and optimization of fluid flow, mass and heat transfer, and related phenomena (e.g. chemical reactions) that may simultaneously take place in a complex system (Liaw, Gu *et al*. 1997). Computers are used to perform millions of calculations required to simulate the interactions of fluids and gases with the complex surfaces used in engineering.

In a CFD Model of a battery, the dynamic governing equations are solved with respect to time, space, and all the physical time and space dependent properties. Acid concentration and potential distribution across the cell, for instance, can be obtained. Therefore such a modelling is able to give a very good understanding to battery parameters and detailed characteristic of battery dynamics.

3.2.3. Equivalent Circuit Model

An equivalent circuit refers to the simplest form of a circuit that retains all of the

electrical characteristics of the original (and more complex) circuit. In its most common form, an equivalent circuit is made up of linear, passive elements. However, more complex equivalent circuits are used to approximate nonlinear behaviours of the original circuit as well.

In electrical engineering, it is often useful to use an equivalent circuit model to describe the non-ideal operation of a device. For electrical engineers, electrical models are intuitive, useful, and easy to handle, especially when they can be used in circuit simulators and alongside application circuits.

3.2.4. Discussion of Different Battery Model Methods

The electrochemical model focuses on the electrochemical reactions and the activities in the battery, which is very popular in the applications for the constructional and design purpose. However, many electrochemical factors contained in the electrochemical model are irrelevant to the external circuit, and some of the important parameters like the internal resistance are hard to describe in an electrochemical model. Therefore this model technology is not able to meet the project **Requirement 1**. As the calculations in the electrochemical model are not complicated, **Requirement 2** can be therefore satisfied by an electrochemical model of battery. **Requirement 3** might be difficult to obtain for an electrochemical model because the understanding of the outputs for an electrochemical model usually need some background knowledge of the battery chemistry. As a result the electrochemical model is not chosen for the project.

Physical models can give good understanding to the battery important parameters so that **Requirement 1** of the project can be satisfied. The **Requirement 3** can be also met as the terminal voltage can be calculated as the output with the knowledge of these parameters. One significant disadvantage is that the physical models involves huge amount of calculation in analysis which is quite time consuming. In finite element or CFD methods, a large nonlinear system of equations is solved iteratively, and that could take excessive CPU time, especially for when the system is more than 2 dimensions. As a result, the physical modelling methods cannot meet the **Requirement 2** of fast response required by the project (Esfahanian, Torabi *et al*. 2008).

In an equivalent circuit model, most of the characteristic required by the project can be reached in a reasonable level. It is able to reflect the dynamic behaviour of battery using simple circuit blocks, such as voltage sources, resistors, and capacitors (Chen and Rinc´on-Mora 2006). That is to say, the **Requirement 1** of the project can be satisfied by the equivalent circuit model. And the model simplicity causes its low computational time as **Requirement 2** and therefore it can be suited to the online implementation (Esfahanian, Torabi *et al.* 2008). Additionally, basic battery parameters like internal resistance, terminal voltage, and SOC etc. can be chosen as the main output of the model to meet the **Requirement 3**.

Table 3-1 summarized a comparison of all the three model methods on the satisfaction of the requirements for the project.

Table 3-1 Satisfaction of the Requirements in different Model Methods

	Requirement 1	**Requirement 2**	**Requirement 3**
Electrochemical Model	×	√	×
Physical Model	√	×	√
Equivalent Circuit Model	√	√	√

3.3. Introduction of the Existing Equivalent Circuit Models

Section 3.2 introduced three different types of battery models to serve for different research purposes, each with different features and strengths. It has been shown that the equivalent circuit model that pays attention to the relationship between the internal circuit and the external characteristics can adequately meet all the requirements of the project. Therefore further studies of battery models have been carried out and six equivalent circuit battery models with different merits and complexity are presented, while the technique improvements are briefly described in this section.

3.3.1. Simple Battery Model

The Simple Battery Model is the simplest battery model. As shown in Figure 3-1, this model consists of only ideal battery E_m as the electromotive force of a battery, and a resistor r in series connection as the internal resistance. V_b in the figure is the terminal voltage of the battery.

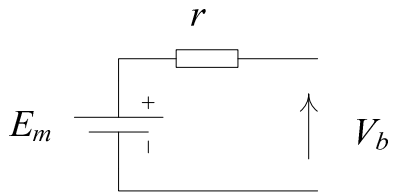

Figure 3-1 Simple Battery Model

The E_m in Figure 3-1 stands for the electromotive force of the battery, while r represents the internal resistance and V_b is the Terminal Voltage. This model is only applicable in some circuits where the state of charge is of little importance because it does not consider the varying characteristic of the internal resistance in different states of charge. The model is often used in circuits where the battery does not have major influences to the circuit analysis. But without being able to describe the battery behaviours in details, this model is not suitable for the research purpose. In the Simple Battery Model, the electromotive force E_m can be obtained by open circuit measurement and r can be calculated by measurement with connecting a load to the battery after taking an open circuit measurement. For a battery with a terminal voltage of 13V and the internal resistance of 0.5Ω, the change of terminal voltage in a Simple Battery Model as the discharge current increases can be given as Figure 3-2

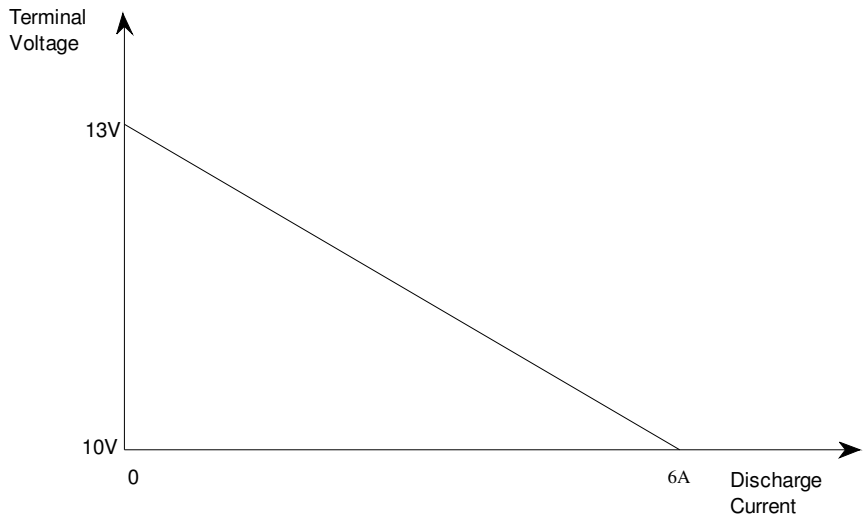

Figure 3-2 I-V chart of the Simple Battery Model

3.3.2. Advanced Simple Battery Model

This model is developed based on the Simple Battery Model and has the same block diagram as the Simple Battery Model. The only difference is that this model employs a variable resistor, which depends on the state of charge (CUN, FIORINA et al.; Durr, Cruden et al. 2006). The relationship between the value of the variable resistance and the state of charge is as follow:

$$r = \frac{R_0}{SOC^a} \tag{3.1}$$

where R_0 is the resistance of the battery when it is fully charged

a is the capacity coefficient

SOC is the state of charge of battery from 0 (completely discharged) to 1 (fully charged)

The most important improvement of this model is that instead of a constant internal resistor, the value of the internal resistance is expressed as equation function of SOC. For the same battery described in section 3.3.1, the I-V chart in different SOCs can be concluded as shown in Figure 3-3.

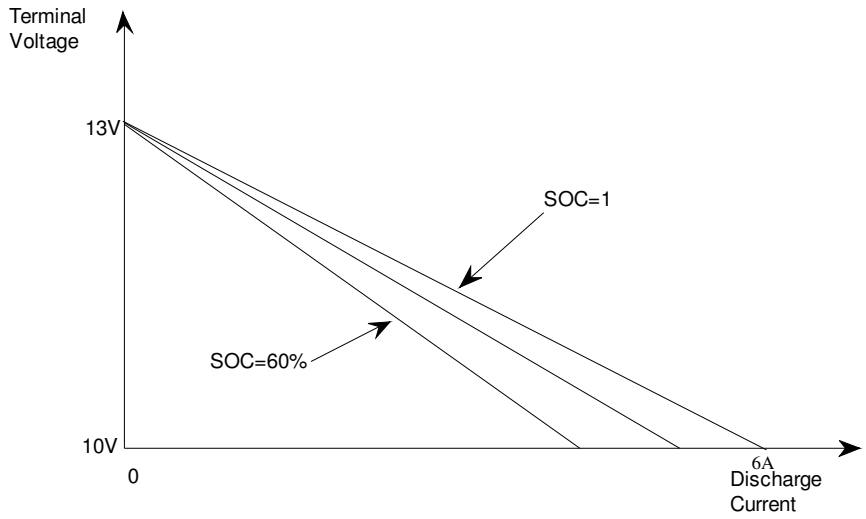

Figure 3-3 I-V Chart in different SOC

3.3.3. Thevenin Battery Model

The previous models do not account for any transient behaviour of batteries. Figure 3-4 shows the gradual change in battery characteristics when external loads are connected or disconnected to the battery.

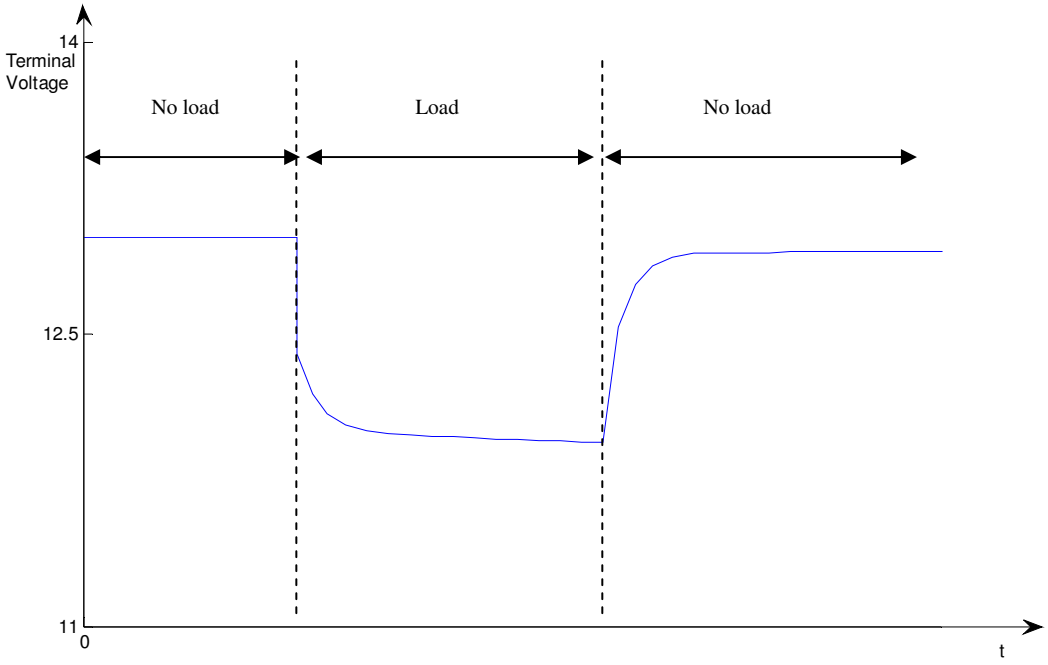

Figure 3-4 Sketch to show battery discharge behaviours in typical tests

Thevenin Battery Model is one commonly used model, which consists of an ideal battery electromotive force (E_m), internal resistance (R_0), overvoltage resistance (R_1) and capacitance (C_1) and the equivalent circuit is shown in Figure 3-5 (Casacca and Salameh 1992; Salameh, Casacca et al. 1992; Chan and Sutanto 2000). C_1 represents the actual capacitance of battery, and R_1 represents the resistance contributed by the contact resistance of the plate and the electrolyte (Durr, Cruden et al. 2006). The capacitance in the Thevenin Battery Model can overcome the trend of terminal voltage shown in Figure 3-4.

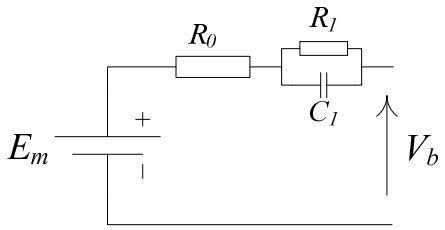

Figure 3-5 Thevenin Battery Model

The main disadvantage of this Thevenin Battery Model is that all the parameter values are assumed to be constant, but, in fact, they are strongly dependent on the state of charge and discharge rate and some other discharge characteristics.

3.3.4. Dynamic Battery Model

This model is developed based on the Thevenin Battery Model. Similar to the improvements made by the Advanced Simple Model comparing with the Simple Battery Model, the most important difference is that it takes into account the non-linear characteristic of the open circuit voltage and internal resistance represented by K / SOC (Jayne and Morgan 1986; Sims 1990).

$$V_b = V_{oc} - (R_b + \frac{K}{SOC})I \tag{3.2}$$

where V_b is the terminal voltage of battery

V_{oc} is the open circuit voltage

R_b is the battery terminal resistor, typically 0.1Ω

K is the polarization constant

I is the discharge current.

3.3.5. Fourth Order Dynamic Model

This is a more accurate and sophisticated model. The current I_p flows through R_p (electrolyte reaction), R_d (Ohmic effect) and its associated leakage capacitance C_d and R_w (waste of energy) and its associated leakage capacitance C_w . Current I_s flowing through the resistor R_s represents the behaviour of self discharge (Gillioli and Cerolo 1990; Chan and Sutanto 2000).

The main drawback of this model, just as its name indicates, is that there are fourth order equations due to consideration of the paralleled R-C blocks in the circuit and therefore it takes more time for the computation. Another drawback is that a number of empirical parameters are contained in the model.

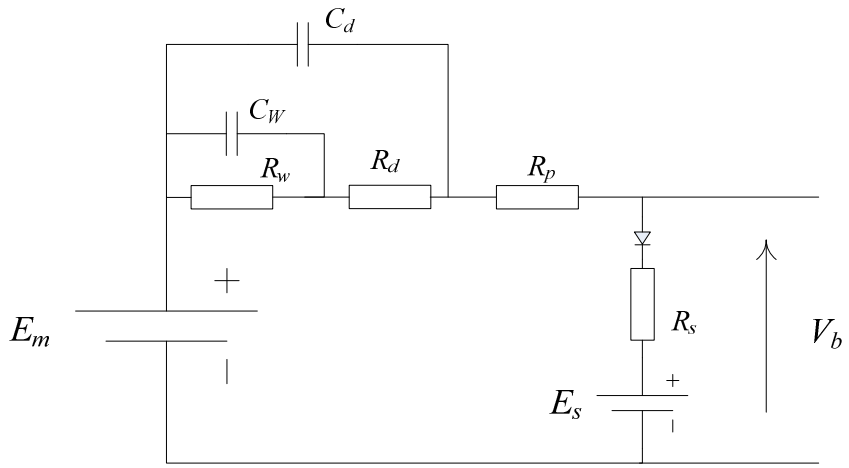

Figure 3-6 Fourth-order Battery Model

3.3.6. Improved Battery Model

The most popular Equivalent Circuit Model used by researchers is the Improved Battery Model (Casacca and Salameh 1992; Salameh, Casacca et al. 1992). This model is simple but meets most requirements for a good battery model. It contains most non-linear characteristics and is linked to the state of charge. Most elements included in this model are the functions of the state of charge or the open circuit voltage, which is also related to the state of charge. The improved model is studied in this chapter and implemented in Matlab/SIMULINK environment.

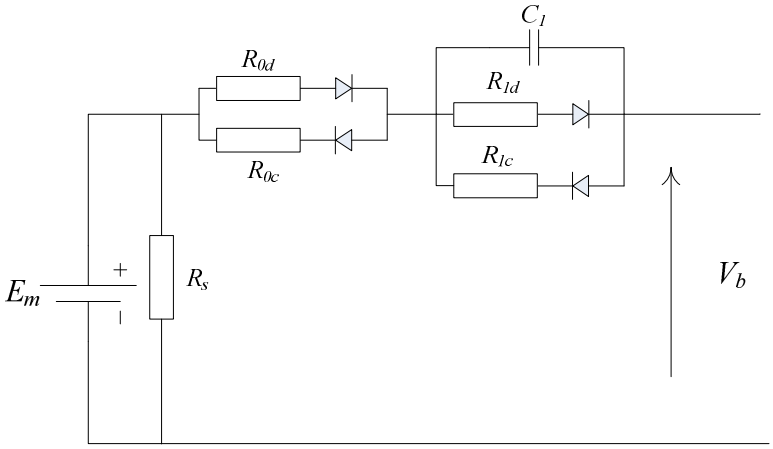

Figure 3-7 Improved Battery Model

3.4. Mathematical Model of the Lead-acid Batteries

As the Improved Battery Model is able to reflect the major dynamic behaviours of a battery and does not take much computation time, it meets the requirements for

the project. Therefore, the mathematical model developed in this project is based on the Improved Battery Model by involving the components of variable voltage sources as the electromotive force (EMF , equal to the open circuit voltage V_{OC}), variable resistors as internal resistance and overvoltage resistance and a capacitor as the capacitance of battery. The description and the detailed analysis of the model are given in this section.

3.4.1. Capacity

Based on the Peukert's law introduced in Chapter 2, the relationship of capacity with different discharge currents is obtained below:

$$\begin{aligned} C_p &= I_1^k t_1 = I_2^k t_2 \\ (I_1 / I_2)^k t_1 &= t_2 \end{aligned} \tag{3.3}$$

And following the definition of battery capacity, the capacity is:

$$\begin{aligned} &C_{I_2} = I_2 t_2 = I_2 (I_1 / I_2)^k t_1 = I_1 (I_2 / I_1)(I_1 / I_2)^k t_1 = (I_1 / I_2)^{k-1} I_1 t_1 = (I_1 / I_2)^{k-1} C_{I_1} \\ &\therefore \quad C_{I_2} = (I_1 / I_2)^{k-1} C_{I_1} \end{aligned} \tag{3.4}$$

where C_p is the one ampere capacity

$C_{I2,}\ C_{I1}$ is the capacity under the discharge current I_2, I_1

k is a constant that related to the battery.

The equation of calculating the capacity by the discharging current can be

obtained through experiments (Ceraolo 2000; Barsali and Ceraolo 2002). An experimental result is given as:

$$C_0(I) = \frac{K_c C_{0*}}{1 + (K_c - 1)(I / I*)^m} \tag{3.5}$$

where $C_{0*} = C_0(I*)$, which stands for the capacity when discharging at the rated discharge rate, usually the nominal capacity C_{10}

K_c is empirical coefficient and is 1.18 for lead-acid batteries,

m is empirical coefficient of 1.20

This equation overcomes the inadequacies of the Peukert's law. The capacity calculated by the Peukert's law in a low discharge current is much larger than that experimentally obtained (Ceraolo 2000).

With the parameters of $C_{0*} = 42Ah, I* = 4.2A, K_c = 1.18, k = 1.20$, the simulation study indicated that the capacities of low discharge rate (<30A) in different equations are quite similar as shown in Figure 3-8.

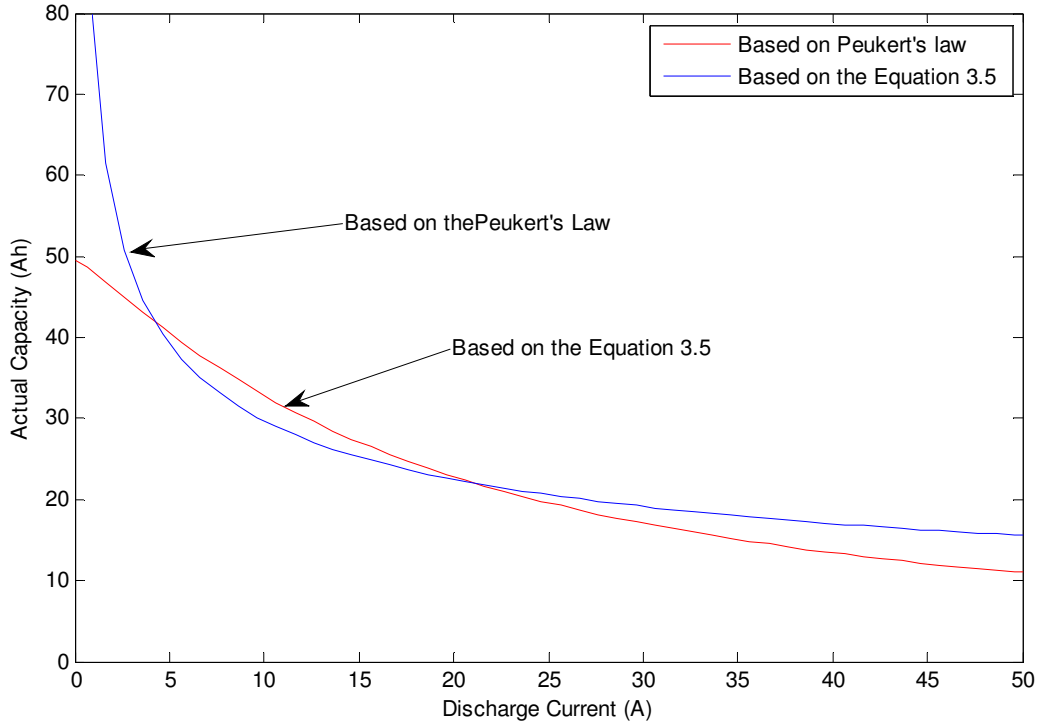

Figure 3-8 Battery Capacity vs. Discharge Current

Variations of the cell temperature also affect the battery capacity. The effect of temperature on the battery capacity is described by the following equation (Ceraolo 2000; Barsali and Ceraolo 2002):

$$C(I,\theta) = C_0(I)\left(1 + \frac{\theta}{-\theta_f}\right)^{\varepsilon} \tag{3.6}$$

where θ_f is the electrolyte freezing temperature and is equal to -40˚C

θ is the cell temperature

$C_0(I)$ is the capacity of battery under the discharge current I at 0˚C

ε is a constant that equals to 1.29

Therefore

$$C(I,\theta)=\frac{K_c C_{0*}\left(1+\frac{\theta}{\theta_f}\right)^{\varepsilon}}{1+(K_c-1)(I/I^*)^m} \tag{3.7}$$

3.4.2. Electric Networks

Figure 3-9 (Ceraolo 2000; Barsali and Ceraolo 2002) shows an adaptation of electric network based on the improved battery model shown in Figure 3-7. The major change of this equivalent circuit is that the self-discharge is not taken into account because the self discharge is usually less than 10% per month in modern technologies, which can be ignored in normal applications.

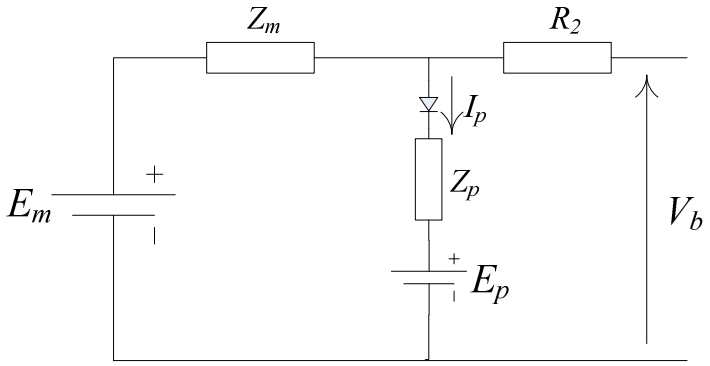

Figure 3-9 Lead-acid Battery Equivalent Network

In the figure, E_m in this the main branch represents the electromotive force of the battery and V_b stands for the terminal voltage. The Z_m in the figure stands for the internal impedance that can be approximated by two R-C blocks.

Battery is an energy storage device, but not all the energy that the battery gets from the charger can be stored when a battery is charged. Part of this energy is lost for different reasons like water electrolysis. A parasitic branch is therefore added to the model to represent the energy loss. This part is claimed to work only when the battery is being charged (Ceraolo 2000; Barsali and Ceraolo 2002). In this project, the current of the parasitic branch I_p in the figure can be described as an equation of the voltage of the parasitic branch V_{PN} instead of a simple resistor R_p because of the nonlinear character of the parasitic branch. This issue will be discussed in later sections.

As a result of these factors, an equivalent electric network of in Figure 3-9 is designed as shown in Figure 3-10, in which C_1, R_1 and R_0 are the elements of the internal impedance Z_m. It is used in the whole project as the electric network of mathematical model.

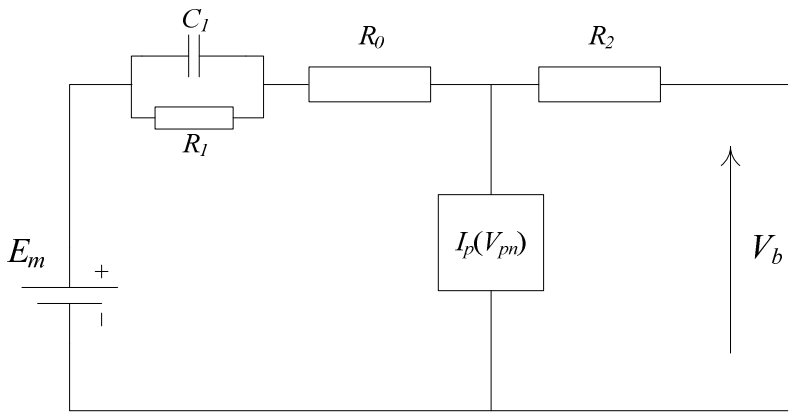

Figure 3-10 The Equivalent Network with the Approximated Z_m

3.4.3. State of Charge and Depth of Discharge

In Chapter 2, Equations 2.7 and 2.8 show the definitions of SOC and DOC of a battery. In the model, the nominal capacity can be treated as $C(0,\theta)$ while the actual capacity is $C(I_{avg},\theta)$, therefore:

$$SOC = 1 - Q_e / C(0,\theta) \tag{3.8}$$

$$DOC = 1 - Q_e / C(I_{avg},\theta) \tag{3.9}$$

where $Q_e(t) = \int_0^t I(\sigma)d\sigma$ is the charge already drained from the battery

$C(0,\theta)$ is the nominal capacity of battery

$C(I_{avg},\theta)$ stands for the actual capacity under the specific discharge current.

3.4.4. Electromotive Force of the Battery

The electromotive force of a battery, which is E_m in Figure 3-10, is the difference between the electric potential of the two electrodes and can be calculated by the Nernst's equation (Eq 2.6)

$$EMF = 2.041 + 0.0296 \log_{10} \frac{\alpha(H^+)\alpha(SO_4{}^{2-})}{\alpha^2(H_2O)}$$

This equation gives a description of the electromotive force by the activity of different matter in the sulphuric acid, which is described as 'α'. When the battery

is being charged or discharged, the electrolyte concentration changes and the activity value of H^+, SO_4^{2-} and H_2O in the Nernst's equation changes, which can be found by the study of battery, that is, the EMF of battery will change as the result of the change of state of charge. The relationship between SOC and the activity α is unknown, but it is obviously that when the state of charge increases, the quotient of $\frac{\alpha(H^+)\alpha(SO_4{}^{2-})}{\alpha^2(H_2O)}$ also increases. This shows that the EMF rises when the state of charge is increasing.

From the literatures (Ceraolo 2000; Barsali and Ceraolo 2002), the electromotive force is described simply as the following equation:

$$E_m = E_{m0} - K_E(273+\theta)(1-SOC) \tag{3.10}$$

where E_{m0} and K_E are constants for a battery

θ is the temperature of the cell

SOC is the state of charge of the battery

3.4.5. Internal Resistance of a Battery

The resistances of a battery as shown in Figure 3-10 can be calculated by the equations (Ceraolo 2000; Barsali and Ceraolo 2002):

$$R_0 = R_{00}[1 + A_0(1-SOC)] \tag{3.11}$$

$$R_1 = -R_{10}\ln(DOC) \tag{3.12}$$

$$R_2 = R_{20} \frac{e^{[A_{21}(1-SOC)]}}{1+\exp(A_{22} I_m / I^*)} \tag{3.13}$$

where A_0, A_{21} and A_{22} are constants for a battery, while R_{00}, R_{10}, R_{20} are parameters related to the SOH, which will be discussed in later chapters. For the model, $R_{20} \approx 0$ and can be omitted when a battery is discharging.

Therefore the internal resistance of a cell when discharging is:

$$r = R_0 + R_1 = R_{00}[1 + A_0(1 - SOC)] - R_{10} \ln(DOC) \tag{3.14}$$

3.4.6. The Behaviour of Parasitic Branch

When the battery is being charged, there are some losses, as represented by the parasitic current. This current depends on the electrolyte temperature and the voltage at the parasitic branch (Ceraolo 2000).

Because the behaviour of parasitic branch is non-linear, Tafel gassing-current relationship is used instead of a simple resistance R_p (Ceraolo 2000):

$$I_p = V_{PN} G_{P0} \exp\left[\frac{V_{PN}}{V_{P0}} + A_p(1 - \frac{\theta}{\theta_f})\right] \tag{3.15}$$

where I_p is the current of the parasitic branch

V_{PN} is the voltage of the parasitic branch

G_{P0} is a constant in seconds

V_{P0} is a constant in volt

A_p is a constant

θ is the electrolyte temperature

θ_f is the electrolyte freezing temperature and is equal to -40˚C

When the battery is being discharged $I_p \approx 0$, the parasitic branch could be omitted from the model in simulation, if the charging behaviour is not necessary to discuss.

3.4.7. Main Branch Capacitance

In the electric network of the model, there is an R-C circuit as shown in Figure 3-11:

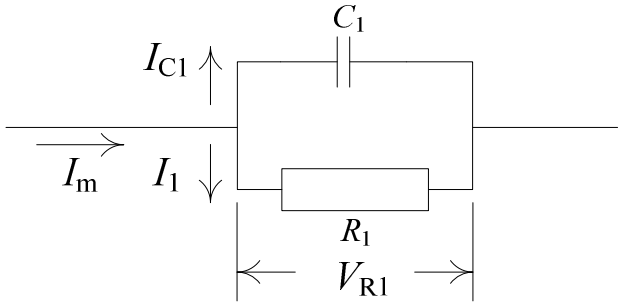

Figure 3-11 R-C block

where I_m is the discharge current

I_{C1} is the current flow through the capacity branch

I_1 is the current of R_1

V_{R1} is the voltage over the R-C block

This branch can be solved by:

$$V_{R1} = R_1 \cdot I_1 = R_1(I_m - I_{C1}) = R_1(I_m - C_1 \frac{dV_{R1}(t)}{dt}) \tag{3.16}$$

$$R_1 C_1 \frac{dV_{R1}(t)}{dt} + V_{R1}(t) = R_1 I_m(t) \tag{3.17}$$

This is the differential equation that represents the main branch behaviour. Laplace transform is employed to solve this problem.

$$R_1 \cdot C_1 \cdot S \cdot V_{R1}(s) = R_1 \cdot I_m(s) \tag{3.18}$$

$$V_{R1} = \frac{R_1 \cdot I_m(s)}{R_1 C_1 S + 1} \tag{3.19}$$

$$G(s) = \frac{V_{R1}}{I} = \frac{R_1}{1 + R_1 C_1 S} = \frac{\left(\frac{1}{C_1}\right)}{\left(\frac{1}{R_1 C_1} + S\right)} \tag{3.20}$$

where $R_1 C_1 = \tau$ is the time constant that represents the double layer capacitance. When the current has a shape like a step, and the initial voltage of the capacitor is equal zero the solution in time becomes:

$$V_{R1}(t) = R_1(1 - e^{-\frac{t}{\tau}}) I_m \tag{3.21}$$

It is obviously that this equation is the typical form of the voltage with an R-C circuit.

3.4.8. Thermal Behaviour of a Battery

When the battery is charging, or discharging, there is a current flow through the battery, so that it produces heat due to the Joule's law:

$$P_s = I_p \cdot V_{PN} + V_{R2} \cdot I + V_1^2 / R_1 + I^2 \cdot R_0 \tag{3.22}$$

When discharging, the parasitic branch and R_2 are omitted, the equation becomes:

$$P_s = V_{R1}^2 / R_1 + I^2 \cdot R_0 \tag{3.23}$$

The dynamic equation of cell temperature and the power is (Ceraolo 2000):

$$C_\theta \frac{d\theta}{dt} = \frac{\theta - \theta_a}{R_\theta} + P_s \tag{3.24}$$

where C_θ is the thermal capacitance

R_θ is the thermal resistance between the battery and the environment

θ is the cell temperature and θ_a is the environment temperature

3.5. Mathematical Model of the Lead-acid Batteries

Considering the behaviour of capacity, state of charge and depth of discharge, electromotive force and internal resistance, an Improved Battery Model based on the equivalent circuit shown in Figure 3-10 was introduced in previous sections. The battery model for the complete discharging progress can be derived as the following equations:

$$C(I,\theta) = \frac{K_c C_{0^*}(1+\frac{\theta}{\theta_f})^{\varepsilon}}{1+(K_c-1)(I/I^*)^m} \tag{3.25}$$

$$Q_e(t) = \int_0^t I(\sigma)d\sigma \tag{3.26}$$

$$SOC = 1 - Q_e / C(0,\theta) \tag{3.27}$$

$$DOC = 1 - Q_e / C(I_{avg},\theta) \tag{3.28}$$

$$E_m = E_{m0} - K_E(273+\theta)(1-SOC) \tag{3.29}$$

$$R_0 = R_{00}[1 + A_0(1-SOC)] \tag{3.30}$$

$$R_1 = -R_{10}\ln(DOC) \tag{3.31}$$

$$C_1 = \frac{\tau}{R_1} \tag{3.32}$$

$$V_{R1}(t) = R_1 \cdot (1 - e^{-\frac{t}{\tau}}) \cdot I \tag{3.33}$$

$$P_s = V_{R1}{}^2 / R_1 + I^2 \cdot R_0 \tag{3.34}$$

$$C_\theta \frac{d\theta}{dt} = \frac{\theta - \theta_a}{R_\theta} + P_s \tag{3.35}$$

$C(I,\theta)$ in the equations is the expression of capacity of battery when discharging under the discharge current I and at a temperature of θ. C_{0*} stands for the capacitance when discharging at the rated discharge current I*, while parameters θ_f and ε are constants in this model. $Q_e(t)$ represents the charge already consumed, while the equation of E_m indicates the mathematical description of electromotive force corresponding to the SOC and the cell temperature, in which E_{m0}, K_E are constants for a battery. R_{00}, R_{10} are parameters related to the SOH, and the discharge current can also affect them. τ in the equations are the time constant of the R-C circuit, which represents the time it takes the system's step response to reach $(1-1/e \approx 63\%)$ of its asymptotic value. The last two equations represent the thermal dynamic of battery, in which P_s is the Joule heat generated by the internal resistance, C_θ is the thermal capacitance and R_θ is the thermal resistance between the battery and the environment.

3.6. Summary and Discussion

The Improved Battery Model based on the electric equivalent circuit is presented in this chapter and it is proved that it can satisfy all the three requirements to serve the project objectives. This battery model consists of a variable voltage source, several R-C blocks and a parasitic branch as its electric network, and the elements are described as a variable related to the capacitance, the charge consumption and

the cell temperature as well.

However, experimental tests show that the behaviour of the battery is much more complicated can be represented by this equivalent circuit model. For example, the internal resistance varies when discharging under different current and the time constant of the R-C circuit at the beginning and end of discharge as well. Therefore the model has to be improved. The next chapter overcomes these problems found in the experimental tests and some improvements of the model are described.

Chapter 4
Experimental System Set up and Improved Battery Model Simulation Implementation

Experimental tests based on a 12V-1.3 Ah lead-acid battery are carried out and the test system is introduced at the beginning of this chapter. Some of the characteristics of the battery can be found in the tests, which has shown that the battery model described previously is not accurate enough and improvements have to be implemented into the model. This chapter will focus on the analysis of the battery characteristics and the description of the improvements implemented. In the last part of this chapter, a finalised version of the battery model used in this project is given and implemented in the Matlab/SIMULINK environment for simulation study.

4.1. The Experimental System

In this experimental test system, a variable resistor is used as the load of the battery. Three sensors are employed in the whole experiment process: two current sensors and one voltage sensor. The equivalent circuit of the test rig designed for the research purpose is shown in Figure 4-1:

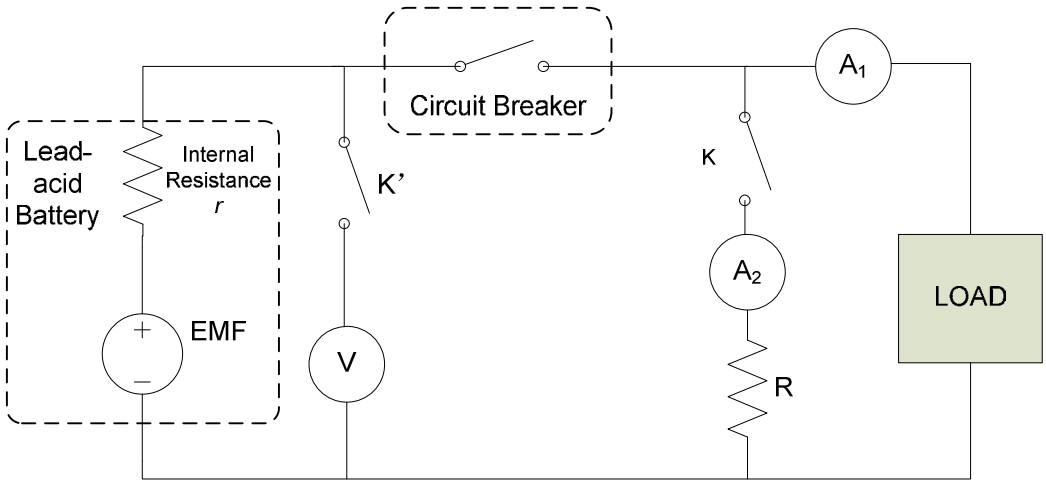

Figure 4-1 Equivalent Circuit of the Experimental Test Rig

In this figure, the ideal voltage source EMF accompanying with the internal resistance *r* acts as a lead-acid battery with 6 cells (12V), the terminals of the battery are connected in parallel to a voltage sensor. Switch K' is employed to control the voltage sensor connection, so that the sensor can be disconnected from the battery when the experiment is not being in progress to avoid an unnecessary discharge. The circuit break in Figure 4-1 can be used as a main controller, which decides whether the load is engaged to the battery to discharge or not. Switch K in the experiment is to vary the load of the system. This experimental test system is mainly designed for two different experimental tests of a battery in this study: constant-impedance load discharge and two-load discharge. Figure 4-2 shows the actual laboratory test rig used in the project.

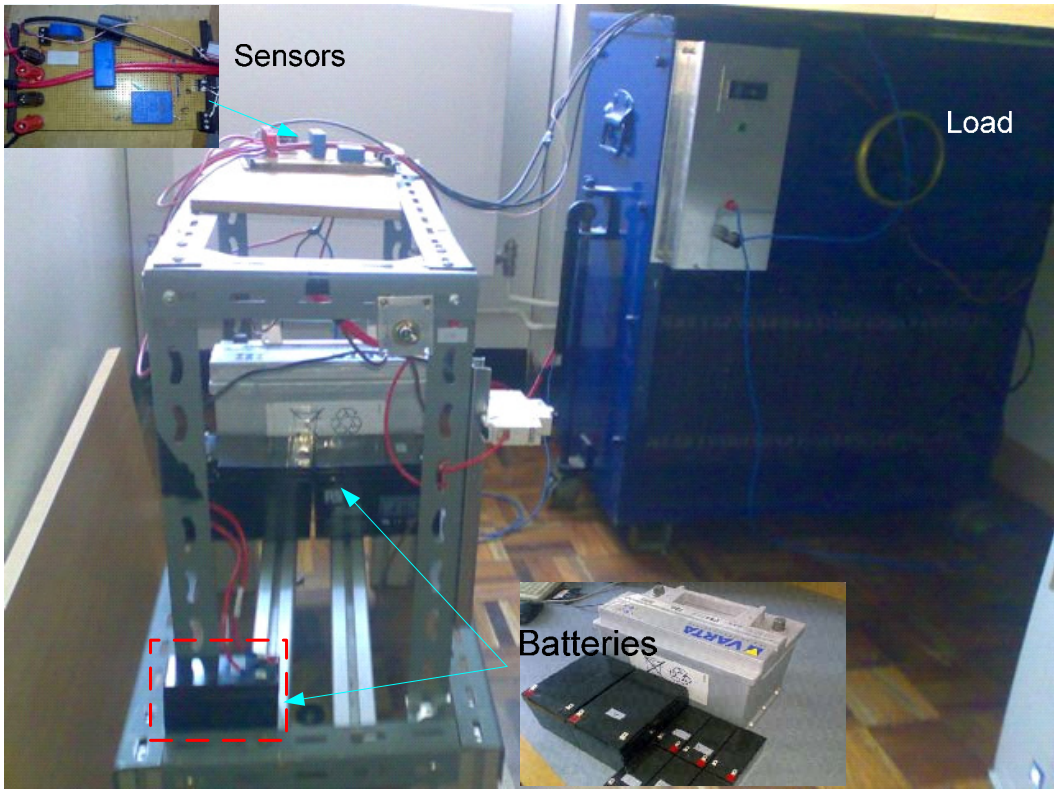

Figure 4-2 Experimental Test Rig

The data is collected and recorded every half second by a data acquisition card PCI-6251 from National Instruments with the software environment of LabVIEW and a 12V-1.3Ah lead-acid battery (marked in the red-dashed square in Figure 4-2) is employed in the project as test batteries for the battery performance study.

4.2. Improvements of the Battery Model

Figure 4-3 and Figure 4-4 show the typical data collected from the experimental test rig. Figure 4-3 is the result of a constant-impedance load discharge test, with a discharge current of 0.75A approximately and Figure 4-4 shows two-load discharge with the discharge currents of 0.75A and 1.2A respectively.

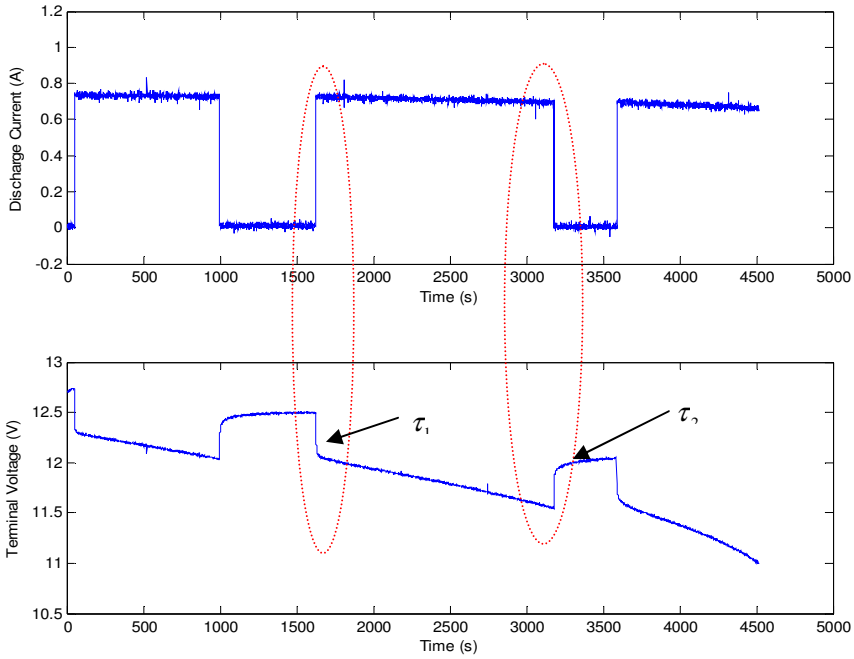

Figure 4-3 Test of constant-impedance load discharge, top figure shows the discharge current of the experimental test and the bottom one shows the terminal voltage. τ_1 is the time parameter of the R-C block at the beginning of the discharge and τ_2 is that when the discharge stopped.

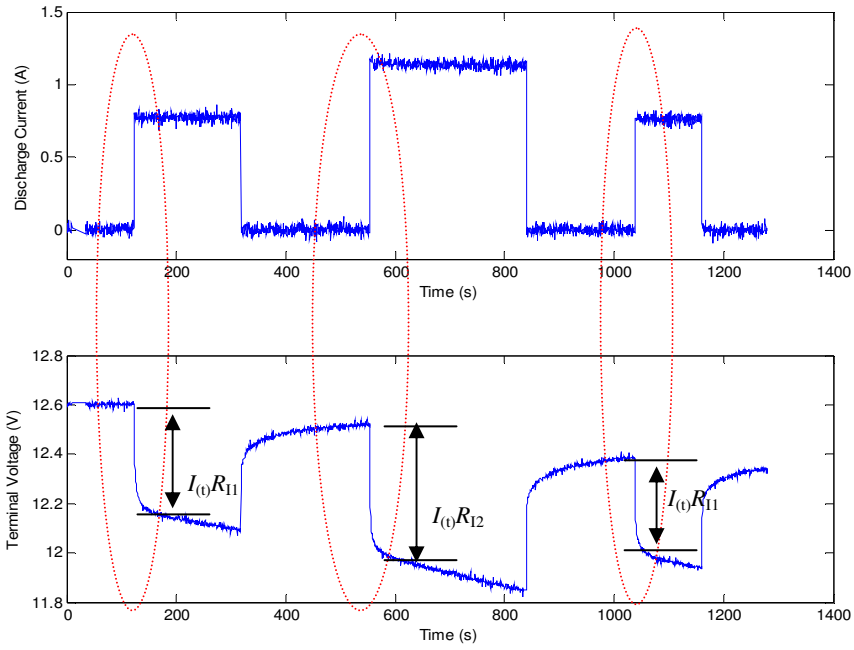

Figure 4-4 Test of two-load discharge, top figure shows the discharge current of the experimental test and the bottom one shows the terminal voltage. $I_{(t)}R_{I1}$ and $I_{(t)}R_{I2}$ represent the voltage drop across the internal resistance value under different discharge current

4.2.1. The Change of τ in Different Charge Status

From analyzing these figures, it is easy to find that it takes quite a long time for the battery to have the steady terminal voltage when the discharge of battery stops and it is longer than the time taken from the beginning of the discharge. This difference means that when the battery starts to discharge, the time parameter $\tau = R_1 C_1$ in the main branch equation (3.32) is not equal to that when the discharge has just stopped. In Figure 4-3, it is shown that when the discharge stops, the time parameter τ is longer than that when the discharge starts.

As a result of this experimental feature, a switch is employed to implement the change of time parameter to match those described in the mathematical model of the battery. The switch is used to control the value of the time parameter τ in different discharge currents. When the battery is discharging, the discharge current is a positive value, and the time parameter τ is equal to τ_1. When the battery is not discharging, the discharge current is equal to 0 in theory, and the time parameter has a different value τ_2.

Although the discharge current should be equal to 0 theoretically, it is hard to achieve this in the real experimental measurement because of the inaccuracy of the current sensor reading due to the inaccuracy occurred in the power supply to the sensor. Therefore, the trigger of the switch in the model is set to be 0.1 A, that is, when the discharge current is greater than 0.1 A, the time parameter is set to be τ_1 as the battery is in its discharging segment. By contrast, the value of time

parameter is set to be τ_2 and the discharge current is considered as the error caused by the sensors when that current is less than 0.1 A.

4.2.2. Analysis in Variations of the Internal Resistance

Another important issue found through analyzing the experimental test result is that the internal resistance for a specific battery in a specific state of health (SOH) is not a constant when the discharging current changes. This difference is more significant than the effect caused by the state of charge.

For example, in the two-load discharge results shown in Figure 4-4, when the battery is not discharging, the initial voltage is equal to the electromotive force (EMF_1). When the battery began to discharge at the discharge current I_1, the terminal voltage dropped to V_1. After the discharge stopped for a while, the value of the terminal voltage is equal to the electromotive force (EMF_2) at that state of charge (SOC_2). Then the discharge of the battery starts again at a current of I_2, and the terminal voltage dropped to V_2. The discharge progress is then stopped for certain of a time period to get the steady terminal voltage (EMF_3) at that state of charge (SOC_3). After that, the test of discharge at the $I_3 = I_1$ was repeated again and get another terminal voltage of V_3. The last discharge test is done to provide the evidence for the fact that this change in the internal resistance is not caused by the change of the state of charge (SOC).

The value of electromotive force in a discharging battery is equal to the sum of the terminal voltage and the voltage that the internal resistance takes, that is,

$EMF_n = V_n + r_n \cdot I_n$.

Therefore the internal resistance can be calculated by:

$$r_n = \frac{EMF_n - V_n}{I_n} \tag{4.1}$$

From the data collected in the experiment, the key parameter values for the graphs shown in Figure 4-4 can be found as listed in Table 4-1.

Table 4-1 Approximate Internal Resistance Calculating

n	1	2	3
Electromotive Force (EMF_n)	12.60V	12.52V	12.38V
Discharge Current (I_n)	0.78A	1.14A	0.76A
Terminal Voltage (V_n)	12.19V	12.03V	11.97V

Substituting these values into Equation 4.1, the internal resistance can be calculated: $r_1 = 0.526\Omega$; $r_2 = 0.430\Omega$; $r_3 = 0.539\Omega$

This change of the internal resistance can cause quite a significant effect in the discharge progress. This problem can be possibly solved in a number of ways. One possible choice is to find a curve of the internal resistance change and the discharge current for a specific battery after a certain numbers of experimental tests. But this method needs huge efforts in conducting experimental tests and the result is not very meaningful for the project considering the time cost. Another possibility is to conduct the experimental tests with a constant load. Therefore, the change of internal resistance caused by the change of discharge current could be ignored. As a result, in the whole process of this project, the same load is

employed either in the constant-impedance load discharge or in the two-load discharge tests.

In order to implement the different internal resistance value when discharging under different load, a switch that can control the parameters R_{00} and R_{10} is employed. This switch is controlled by the discharge current, which is the main input of the mathematical model. In the two-load discharge tests, when the switch K in Figure 4-1 is switched off, there is only one load is connected to the battery terminals, and the discharge current is lower, the values of R_{00} and R_{10} are switched to the first set of parameters R_{001} and R_{101}. To the contrast, when K is switched on, the discharge current is higher, and the values are switched to the second set R_{002} and R_{102}

4.2.3. Improved Lead-Acid Battery Mathematical Model

From the model described in Chapter 3 and the improvements studied in this chapter, the mathematical model of lead-acid battery when discharging in different discharge currents can be described as the following equations:

$$C(I,\theta) = \frac{K_c C_{0^*} (1 + \frac{\theta}{\theta_f})^{\varepsilon}}{1 + (K_c - 1)(I / I^*)^m} \tag{4.2}$$

$$Q_e(t) = \int_0^t I(\tau) d\tau \tag{4.3}$$

$$SOC = 1 - Q_e / C(0,\theta) \tag{4.4}$$

$$DOC = 1 - Q_e / C(I_{avg},\theta) \tag{4.5}$$

$$E_m = E_{m0} - K_E(273+\theta)(1-SOC) \tag{4.6}$$

$$R_0 = R_{00}[1 + A_0(1-SOC)] \tag{4.7}$$

$$R_1 = -R_{10}\ln(DOC) \tag{4.8}$$

$$C_1 = \frac{\tau}{R_1} \tag{4.9}$$

$$V_{R1}(t) = R_1 \cdot (1 - e^{-\frac{t}{\tau}}) \cdot I \tag{4.10}$$

$$P_s = {V_{R1}}^2 / R_1 + I^2 \cdot R \tag{4.11}$$

$$C_\theta \frac{d\theta}{dt} = \frac{\theta - \theta_a}{R_\theta} + P_s \tag{4.12}$$

$$R_{00} = \begin{cases} R_{001} & (Load_1) \\ R_{002} & (Load_2) \end{cases} \tag{4.13}$$

$$R_{10} = \begin{cases} R_{101} & (Load_1) \\ R_{102} & (Load_2) \end{cases} \tag{4.14}$$

$$\tau = \begin{cases} \tau_1 & (I > 0.1A) \\ \tau_2 & (I < 0.1A) \end{cases} \tag{4.15}$$

R_{001}, R_{002}, R_{101}, R_{202} and τ_1, τ_2 in the equations stand for different parameter values of R_{10}, R_{20} and τ when the load and charge status changes in order to reflect the improvements described in this chapter. For a two-load discharge test, there are ten important unknown parameters in the equations of the mathematical model, which are unknown for a specific battery: C_{0^*}, E_{m0}, K_E, R_{001}, R_{002}, R_{101}, R_{102}, τ_1, τ_2 and A_0. As the internal resistance R_{00} and R_{10} vary only when the load changes, they can be treated as constants in the constant-impedance load

discharge tests, the key parameters are therefore $C_{0*}, E_{m0}, K_E, R_{00}, R_{10}, \tau_1, \tau_2$ and A_0. In this project, the study of state of health is based on constant-impedance load discharge. The identification of these unknown parameters will be discussed in Chapter 5.

4.3. Simulation Study

The processes described above have been implemented in SIMULINK as a simulation model for computer based analysis. The simulation program consists of two main function blocks: circuit block and thermal block. The structure of the SIMULINK implementation is described in Figure 4-5.

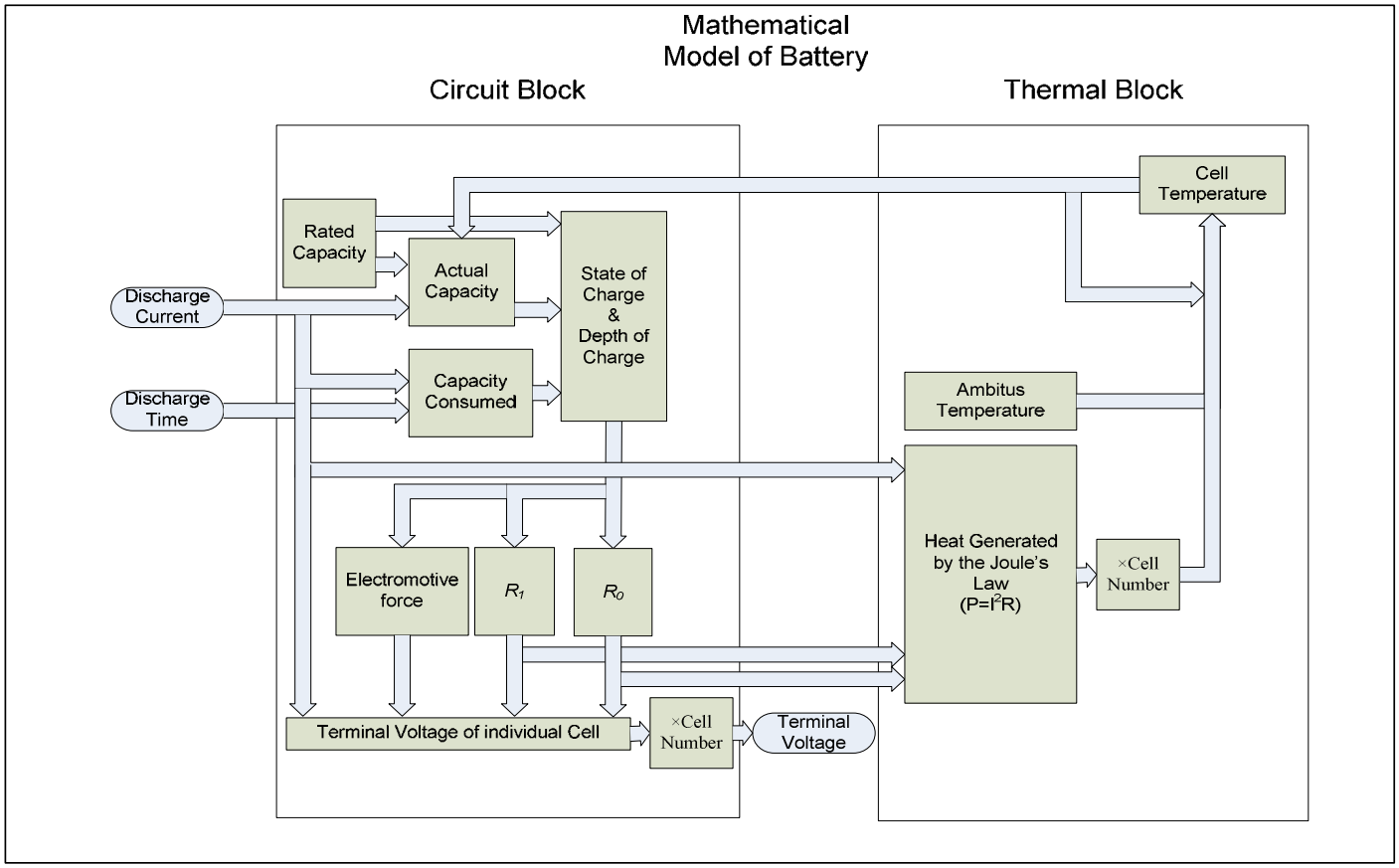

Figure 4-5 Structure of model for SIMULINK Implementation

As shown in the figure, there are mainly two inputs in the model: the discharge current and the discharge time. The actual capacity of battery can be then calculated with the knowledge of rated capacity and the discharge current. The actual capacity is also influenced by the cell temperature. At the beginning of discharge, the cell temperature is the same as the surrounding temperature. Integrating the discharge current with respect to time is the capacity consumed in the discharge progress and then the state of charge and the depth of charge can be obtained. It is shown that the electromotive force and the internal resistance vary as a result of changing in the state of charge and the depth of charge, and the terminal voltage can be calculated.

In the thermal block of the model, the heat generated by the current and the internal resistance are calculated by the Joule's law. Then, this energy is transferred to calculate the thermal temperature of the cell and the cell temperature is given back to the circuit block to affect the actual capacity.

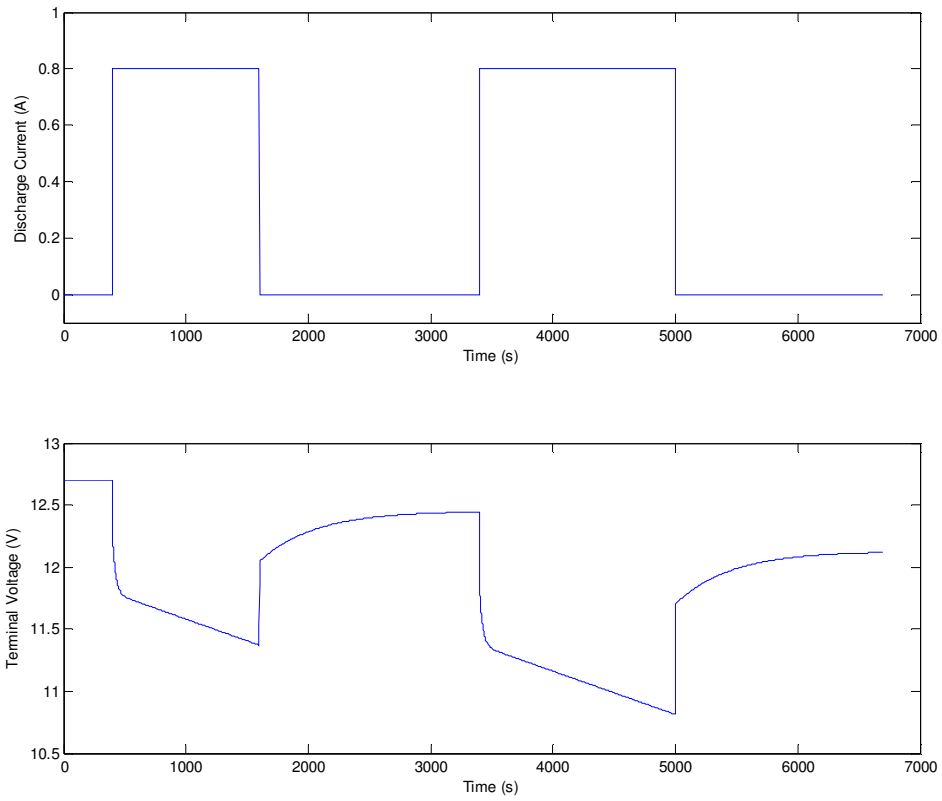

Figure 4-6 Terminal Voltage of Battery (Constant Discharge Current, SIMULINK)

The result in Figure 4-6 shows the terminal voltage of a battery, which discharges under the current of 0.8A in a simulation study. Since the discharge begins, the voltage drops due to the internal resistance and the change of state of charge (SOC) and it climbs up when the discharge stops. However, the voltage changes gradually because of the time parameter τ. This result shows a good qualitative agreement with the experimental test results.

4.4. Summary and Discussion

This chapter introduces the laboratory test system designed for the project and the limitation of the mathematical model described in Chapter 3. Switches on the time parameter τ and the internal resistance parameters R_{00} and R_{10} have been added to the model so that the model is able to represent the change of these parameters found in the experimental tests. The implementation of the model under the Matlab/SIMULINK environment is described and the simulation study shows a good qualitative agreement with the experimental test results.

The next chapter will focus on the identification of those unknown parameters of the battery model that are important for revealing the battery characteristics, including $C_{0^*}, E_{m0}, K_E, R_{00}, R_{10}, A_0, \tau_2$ and τ_1.

Chapter 5
Model Parameter Identification and Model Validation

The identification of the unknown parameters $C_{0^*}, E_{m0}, K_E, R_{00}, R_{10}, A_0, \tau_2$ and τ_1 in the mathematical model will be introduced in this chapter。

5.1. Need for the Optimization Algorithms

In those equations of the battery model described previously, some parameters are unknown and some of them are difficult to derive from physics or engineering principles or to be obtained through experimental tests. Therefore the identification of the model unknown parameters becomes an important part for the project. Parameter identification is an optimization process that adjusts the parameters to enable the simulation results to show the best agreement with the results acquired by the experimental tests. There are many algorithms available for optimization, and the principle of the optimization process for the project is to minimize the objective function. The objective function is formed by the absolute value of the difference between the simulated and experimental results at each time point. The set of parameters to achieve the least value of the objective function is considered to be the fittest set.

There are two basic requirements of the optimization in this project. First of all, as the problem for the solutions trapped to the local minima is a very important and challenging issue in many linear optimization solvers, the optimization algorithm used in this project must be able to find the global minimum. Secondly, the optimization algorithm not only should find the minimum value of the objective function but also can tell the values of the parameters that result in the best fitness, which is needed for the analysis purpose in this project. Finally, the time cost is also an important factor in selection of a suitable optimization algorithm.

It needs to point that the objective here is to identify the unknown parameters of a model with an already known structure. If the objective is to identify or approximate unknown model structures, the selection of optimisation methods will be quite different. In the case of latter, Neural Network, Genetic Programming and Fuzzy Logical will be more suitable choices. To concentrate on the objective of the project, the thesis will focus on optimisation algorithms for parameter identification.

5.2. Overview of the Optimization Algorithms

Brute-force search is the most basic direct search algorithm that is used to find the minimum value. In the brute-force search, the initial guess is the minimum possibility of parameters and increases/decreases. The parameter increases/decreases step by step in each iteration and the best solution can be

searched. This algorithm is the simplest, but its disadvantage is also obvious, that is, it is the slowest optimization method especially when used in the identification of more than two parameters and the results are largely dependent on the initial guesses.

Linear search is an optimization method to solve the linear optimization problem, the preference function of which is linear and the feasible domain is defined by a linear constraint function. The linear constraints define a convex polyhedron geometrically, which is called the feasible region. The algorithm is to construct an admission solution at a vertex of the polyhedron and then along edges of the polyhedron to vertices with successively higher values of the objective function until the optimum is reached.

Besides the basic optimization methods, evolution computation technology is becoming increasingly popular. A range of different evolution computation technologies can solve the optimization problem in this project, including genetic algorithms (GAs), particle swarm optimization (PSO).

Genetic Algorithms are direct search algorithms inspired from the process of evolution in nature: the natural selection. Based on the principle of survival of the fittest, the GAs can produce better and better approximations to the global optimal solution in a number of generations. In each generation, a new group of solutions is created by the fitness level in the problem of every individual in the last generation. The solutions are then bred together to lead to the evolution of individuals.

Particle swarm optimization is a stochastic population-based computer algorithm modelled on swarm intelligence that searches for a solution to an optimization problem in a search space. Based on the social psychological principles, each individual, called 'particle' in PSO, is able to provide information to others and also learn the success from the local best and the global best. The movement of each particle through the search space are guided by these successes and the solution can be found after a number of generations.

It has been proved by Dr. Jianlin in his PhD Thesis (Wei 2007) that both Genetic Algorithm and Particle Swarm optimization are capable of the model parameter identification. But the Particle Swarm optimization is a new algorithm that first described in 1995, and it is not as common as Genetic Algorithm in the research areas.

The purpose of this research work is to find a method for parameter estimation. Genetic algorithms are well proven solution for complicated optimisation problems and have been applied successfully in a range of similar problems (Wei 2007; Wei, Wang et al. 2007). Genetic algorithms are also well suited to problems with many local minima. In the current work, the exact form of the fitness function is unknown and it is therefore important to select a robust technique which can identify good overall solutions. For these reasons GA was selected, to give the best possible chance of satisfying the overall project objectives within the limited timeframe of the project.

5.3. The Study of the Genetic Algorithms

The process of Genetic Algorithm is reviewed in this section to provide an insight into how GAs work, and simulation study of two bench mark functions are carried out.

5.3.1. Working Principle of GAs

There are many methods used to implement a GA process, and usually a GA is at least composed of three common genetic operators: Selection, Crossover and Mutation (Pham and Karaboga 1998). The flowchart of a simple GA process is given in Figure 5-1.

As a preparation to start the optimization process, a GA requires a group of initial solutions as the first generation. The first generation is usually a group of randomly produced solutions created by a random number generator. The population, which is the number of individuals in a generation, should be big enough so that there could be a reasonable amount of genetic diversity in the population. Also, it should be small enough for each generation to be computed in a reasonable period of time using the computer resources available. Typically, a population includes individuals between 20 and 100 (Chipperfield, Fleming et al. 1994A).

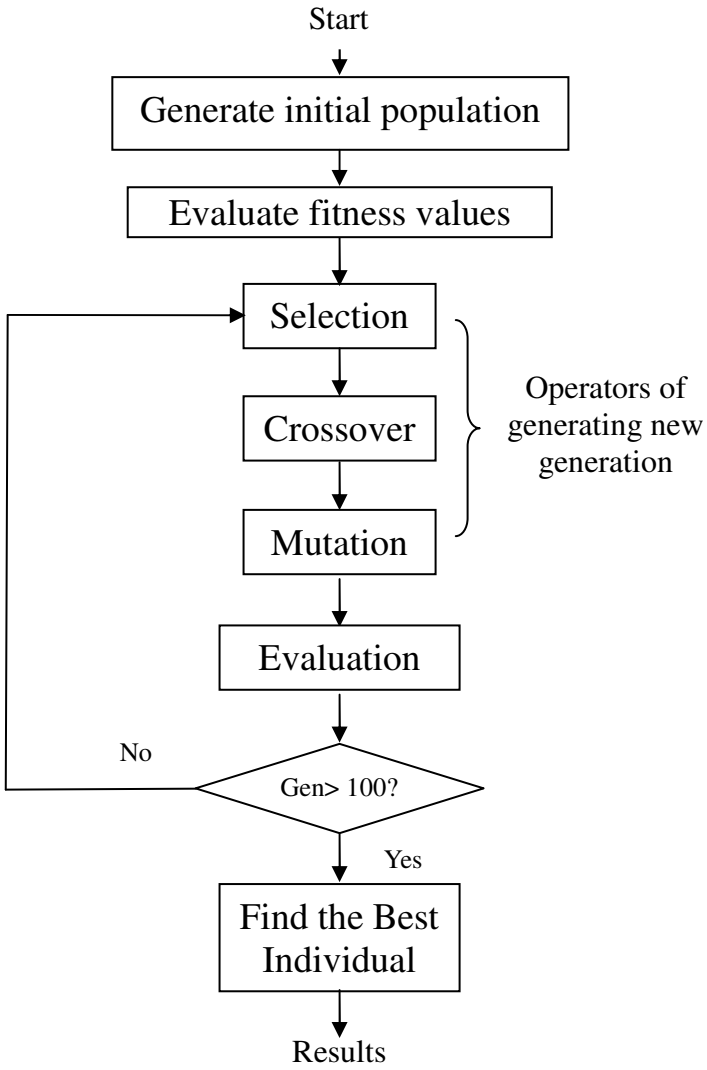

Figure 5-1 Flowchart of a Simple Genetic Algorithm (Pham and Karaboga 1998)

The fitness function is evaluated to measure how close that the individuals fit the desired result. A fitness function could be either complex or simple depending on the optimization problem addressed. In a case of minimization problem, the most fitted individuals will have the lowest numerical value of the associated fitness function.

Individuals are selected according to a fitness-based process. The operator of selection is made up of ranking and selection progress, by which more copies of the individuals that fit the optimization problem better will be produced in the next generation. In GAs, there are mainly two ways to select a new population: Roulette Wheel Selection (RWS) and Stochastic Universal Sampling (SUS).

The individuals will be recombined (crossover) after the selection. This operation is to produce two new individuals from two existing individuals selected by the operator of selection by cutting them at one or more position and exchanging the parts following the cut. The new individuals therefore can inherit some parts of both parents' genetic material. There are usually four ways of doing this: one-point crossover, two-point crossover, cycle crossover and uniform crossover (Pham and Karaboga 1998). Figure 5-2 (a) shows an example of the two-point crossover progress.

Mutation is another operator to produce new individuals. The difference is that the new individual is produced from a single old one. In this operation, the bit values of each individual are randomly reversed according to a specified property. A mutation can also helps the GA to avoid local optimums and find the global best solution. Figure 5-2 (b) represents how the mutation operator works.

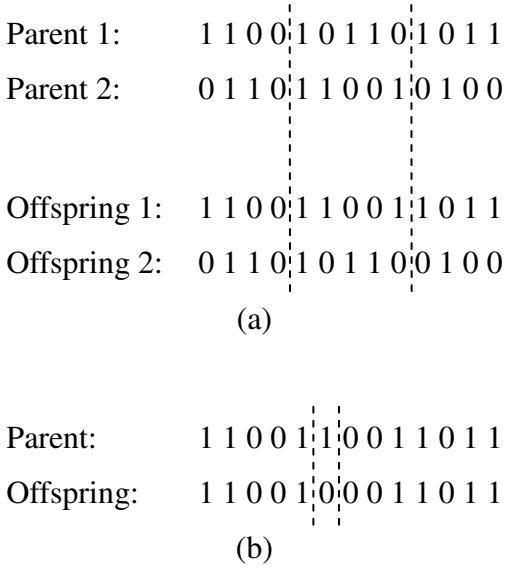

Figure 5-2 (a) Crossover operation; (b) Mutation operation

The group of individuals produced after the mutation is the second generation. Then the fitness value of each individual in the second generation is computed again. This cycle will not stop until the result is close enough or after a certain generation.

Three major Matlab toolboxes are applied in the current market for application purpose, they are: Genetic Algorithms Toolbox V1.2 (Chipperfield, Fleming et al. 1994B), the Genetic Algorithms Optimization Toolbox V1.1 (Houck, Joines et al. 1995), Genetic Algorithm Direct Search Toolbox V1.02 (MathWorks Inc. 2004). In this project, the official toolbox in Matlab form Mathworks Inc. is employed. The property settings for the project based on Dr. Wei's thesis (Wei 2007) are shown in Table 5-1:

Table 5-1 The property settings for Genetic Algorithms

Name of the GA properties	Value of the GA properties
Number of generations	100
Population size	20
Fitness assignment	Rank-base fitness assignment
Selection	Stochastic universal sampling
Crossover	Scattered crossover
Crossover rate	0.7
Mutation function	Uniform mutation
Mutation rate	0.1

Population size specifies how many individuals there are in each generation. With a large population size, the genetic algorithm searches the solution space more thoroughly, and the gives more possibility to return the global minimum. The number of generations specifies the maximum number of iterations for the genetic algorithm to perform. If this number is too low, the genetic algorithm is not able convergence to the global solution. However, either a large population size or a large number of generations can cause the algorithm to run more slowly. The crossover rate and the mutation rate are properties that control the crossover and mutation operator. High rate of these values means that the genetic algorithm has a higher opportunity of producing new offspring, but it can be easy to miss the current best solution if these values are too big.

Initial tests of genetic algorithms on different properties show that the values shown in table 5-1 are able to find an adequate solution. Similar results would be

obtained if the values of the generations and the population size are larger, but costing more CPU time. The crossover rate and the mutation rate would not affect the result significantly if only varies in a small range. But it is impossible to prove that these two values are the best choice due to the strong randomness.

5.3.2. Simulation Studies of Genetic Algorithms

In order to test and demonstrate that Genetic Algorithms are able to meet the requirements of the project, simulation studies have been carried out. Two benchmark functions that are commonly used in evaluating evolutionary computation algorithms are employed for the simulation studies. They are:

1) Rastrigin function

Rastrigin function is a typical example of non-linear multimodal function with many local minima. The problem of looking for the global minimum is quite difficult due to its large search space and its large number of local minima. The function is shown as:

$$f(\vec{X}) = 10 \cdot n + \sum_{i=1}^{n} ({x_i}^2 - 10 \cdot \cos(2\pi \cdot x_i))$$

where n is the dimension of the problem and $x_1 \sim x_n$ are the coefficients to be identified. Figure 5-2 shows a 2-dimensional Rastrigin's function while figure 5-3 is a contour plot of Rastrigin's function shows the alternating maxima and minima.

The global minimum of the Rastrigin's function is $f(\vec{X}) = 0$ when $x_1 = x_2 = \cdots = x_n = 0$.

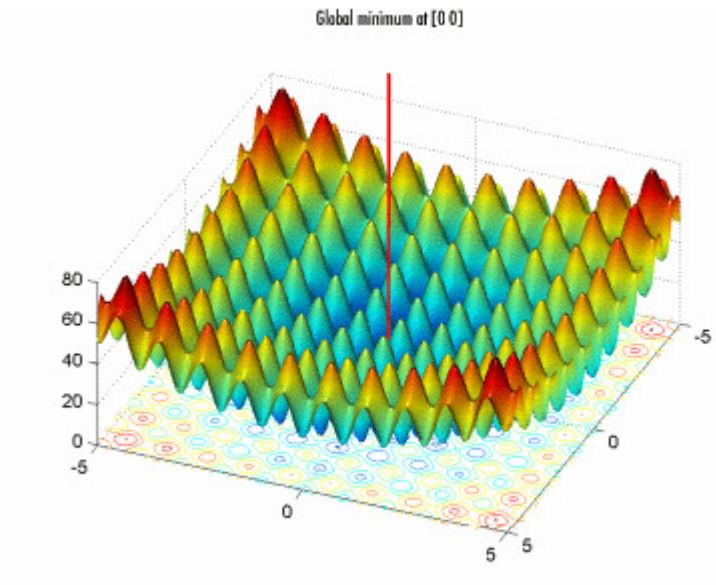

Figure 5-2 2-dimensional Rastrigin's function (MathWorks Inc. 2004)

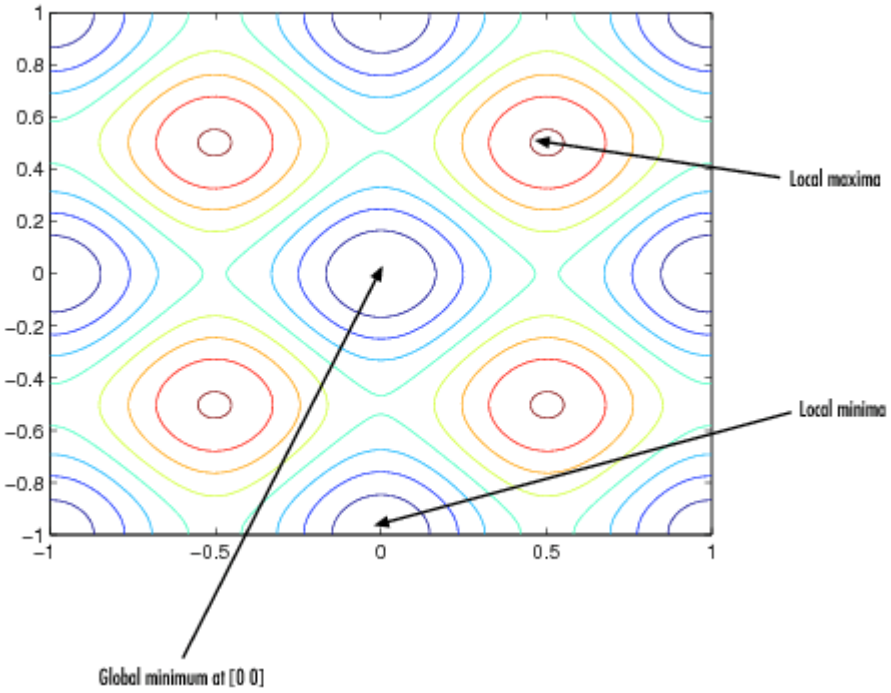

Figure 5-3 Contour plot of Rastrigin's function (MathWorks Inc. 2004)

In the simulation study, a ten dimensional Rastrigin's function is adopted. Figure 5-4 shows the best optimization performance of the Rastrigin's function in each generation. It is shown that after 700 generations, a global optimal value is obtained.

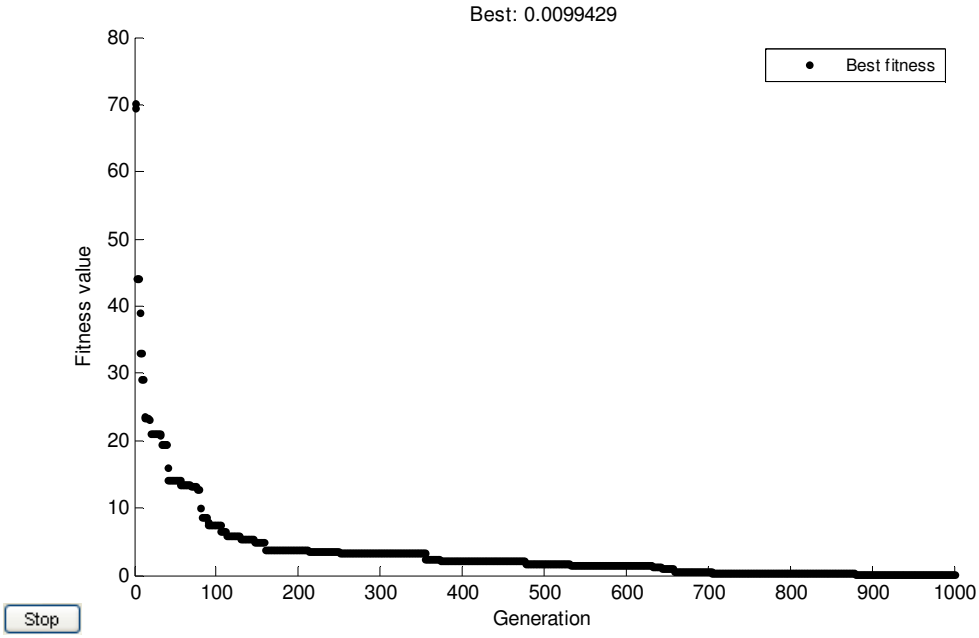

Figure 5-4 GA performance (Rastrigrin's function)

2) Rosenbrock function

Rosenbrock function is another mathematical function used as a test problem for optimization algorithms. The global minimum is inside a long, narrow, parabolic shaped flat valley. To find the valley is trivial, but to converge to the global minimum is difficult. The Rosenbrock function is defined by:

$$f(\vec{X}) = \sum_{i=1}^{n} (100(x_{i+1} - x_i^2)^2 + (x_i - 1)^2)$$

where n is the dimension of the problem, and $x_1 \sim x_n$ are the coefficients to be identified. Figure 5-5 shows a 2-dimensional Rosenbrock function.

The global minimum of the Rosenbrock function is $f(\vec{X}) = 0$ when $x_1 = x_2 = \cdots = x_n = 1$. The same as the Rastrigin's function, a ten dimensional Rosenbrock function is adopted for the simulation study. Figure 5-6 is the GA performance to the Rosenbrock function. It can be found that the optimization converges and get the global optimal value after 300 generations.

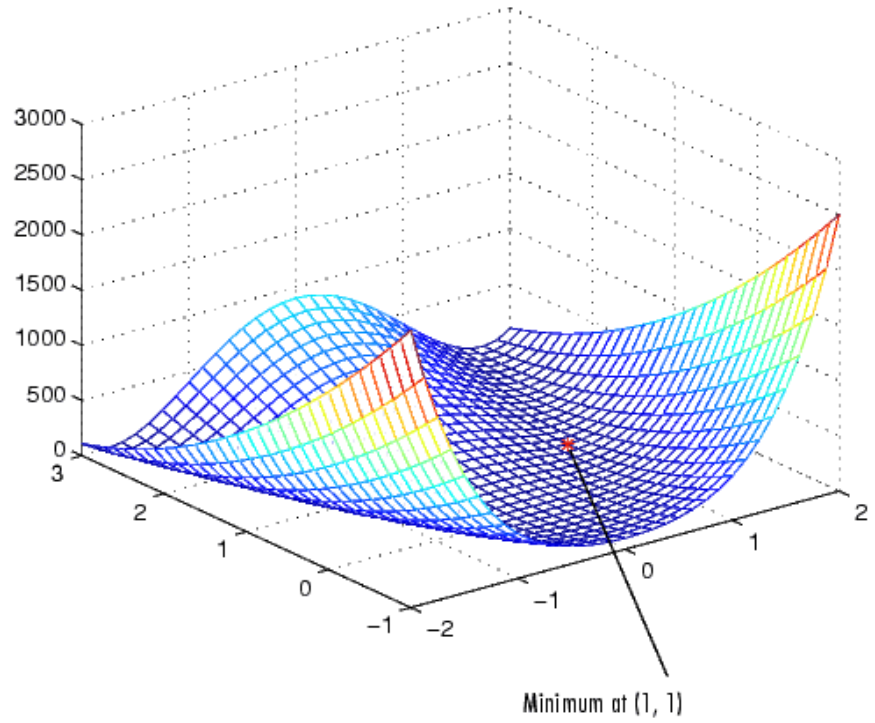

Figure 5-5 2-dimensional Rosenbrock function (MathWorks Inc. 2004)

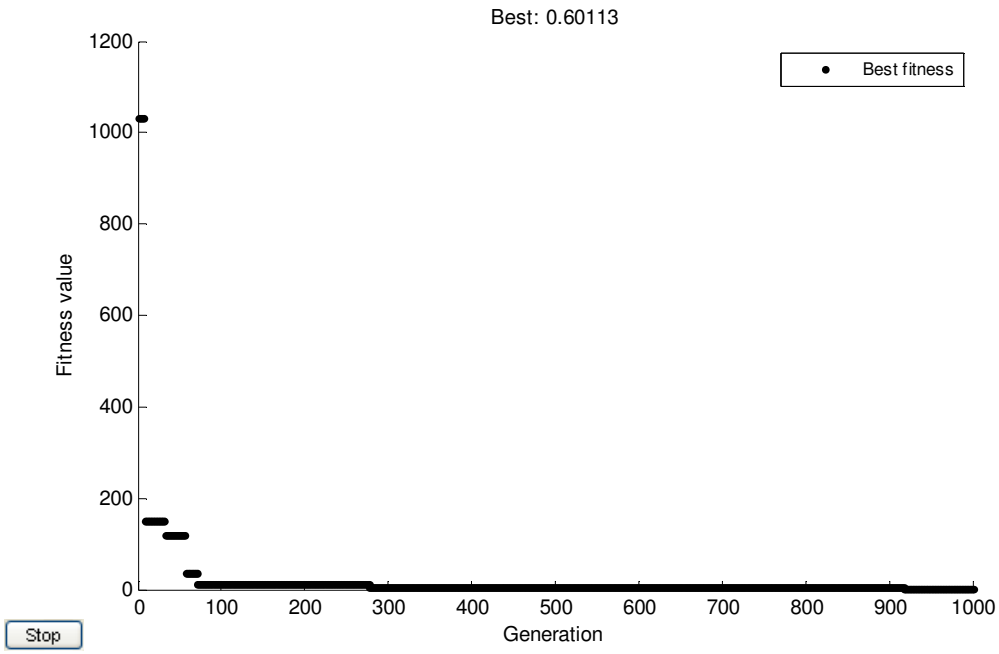

Figure 5-6 GA performance (Rosenbrock function)

5.4. Model Parameter Identification

5.4.1. Implementation of Genetic Algorithms and Experimental Data sets

In this project, the Genetic Algorithm Direct Search Toolbox V1.02 developed by Mathworks Inc. is employed to identify the parameters of the battery model. The process is shown in Figure 5-7.

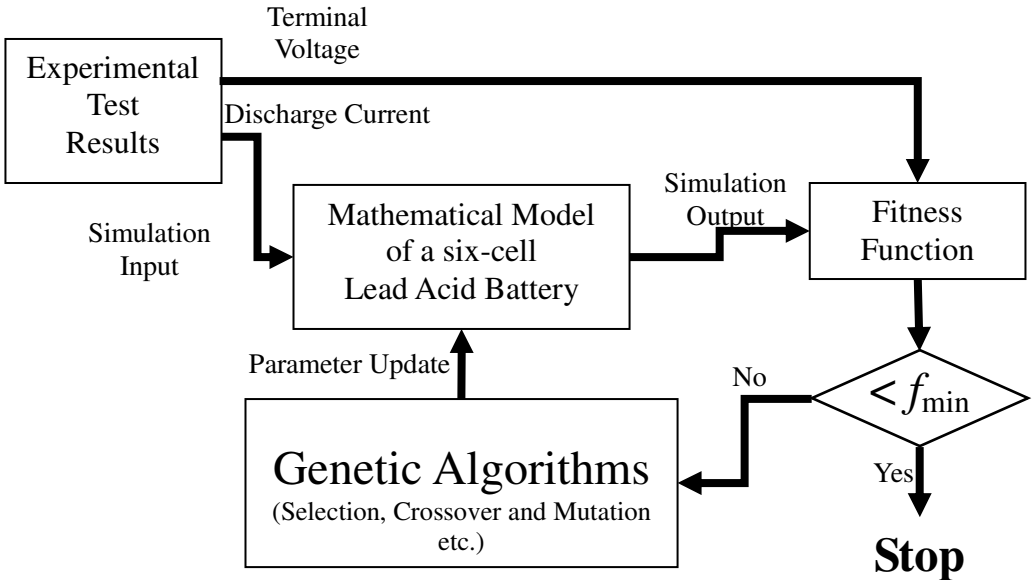

Figure 5-7 Progress of Parameter Identification

The fitness function is used in the project and the parameter identification is to minimize the fitness function, so that the model output can fit the experimental result. The fitness function is given as:

$$fitness = W_1 \cdot \sum_{t_0}^{t_1} abs(V_{\exp} - V_{sim}) + W_2 \cdot \sum_{t_1}^{t_2} abs(V_{\exp} - V_{sim}) + \cdots + W_n \cdot \sum_{t_{n-1}}^{t_n} abs(V_{\exp} - V_{sim})$$

$$= \sum_{t_0}^{t_1} W(t) \cdot abs(V_{\exp}(t) - V_{sim}(t))$$

where $V_{\exp}$ is the experimental terminal voltage data

V_{sim} is the simulated terminal voltage

W_t is the weights of the difference in the simulated and experimental results

This fitness function represents the sum of the error values at each time interval

considered ($t_0 - t_n$). The weight coefficients W_t indicates how important the weighted part is in the optimization and how much it contribute to the optimisation process. Periods with bigger W_t values are more important because the sum of errors will give big value contribution to the fitness function value and the optimisation process will pay more attention to the higher weighted error parts. In the experiments and optimization process, it is found that the results were more important when the discharge of a battery at the stage of stopping. Therefore, the weight in this period is greater than that of the others. The weighting coefficient values in this project are determined by the results of the first several attempts of parameter identification. The period of simulation data that fails to fit the test result means that the weight value is not big enough until the overall performance of simulation is reasonable.

Following the objective fitness function, unknown coefficients of the battery model are identified using experimental data. The mathematical model of a six-cell lead-acid battery in the figure is described in Chapter 4 and the parameters are to be identified by Genetic Algorithms are: $C_{0^*}, E_{m0}, K_E, R_{00}, R_{10}, A_0, \tau_1, \tau_2$.

Three sets of experimental tests have been carried out for the purpose of parameter identification and the validation of the mathematical model. These three experimental results are based on a lead-acid battery with the ideal capacity of 1.3 Ampere-hours under the discharge current of 0.8A.

5.4.2. Parameters of Battery Model

The parameters of the mathematical model of a lead-acid battery are identified using Genetic Algorithms and the predicted battery responses using the identified parameters are compared with the simulated results. One set of typical values of parameters identified are listed in Table 5-2:

Table 5-2 Identified parameters identified by the Genetic Algorithms in the model of 12V-1.3Ah lead-acid battery

Parameter	Value	Parameter	Value
C_{0*}	4819.8 (Amp-Sec)	E_{m0}	2.1465 (V)
K_E	0.001109 (V)	A_0	2.9895
R_{00}	0.01038 (Ohm)	R_{10}	0.12196 (Ohm)
τ_1	210.52 (s)	τ_2	17.565 (s)

Figure 5-8 shows the simulation results using the Improved Battery Model and the change of weights defined for this set of result described in the fitness function. The top subplot of Figure 5-8 shows the weight value of the GA fitness function described before while the middle figure is the discharge current of the experimental test, which is also the input of the mathematical model. In the following test results in this and next chapter, the changes of weight value are similar so they are not shown in the figures.

The blue line marked as “Experimental Terminal Voltage” in the bottom figure represents the measured outputs while the other one (Simulated Terminal Voltage) represents the simulation results. The simulation results are “noisy” because experimental discharge current is used as the input of model in the simulation

progress. It is obviously that Figure 5-8 shows a good overall agreement of the results although some slope when discharging is not perfect.

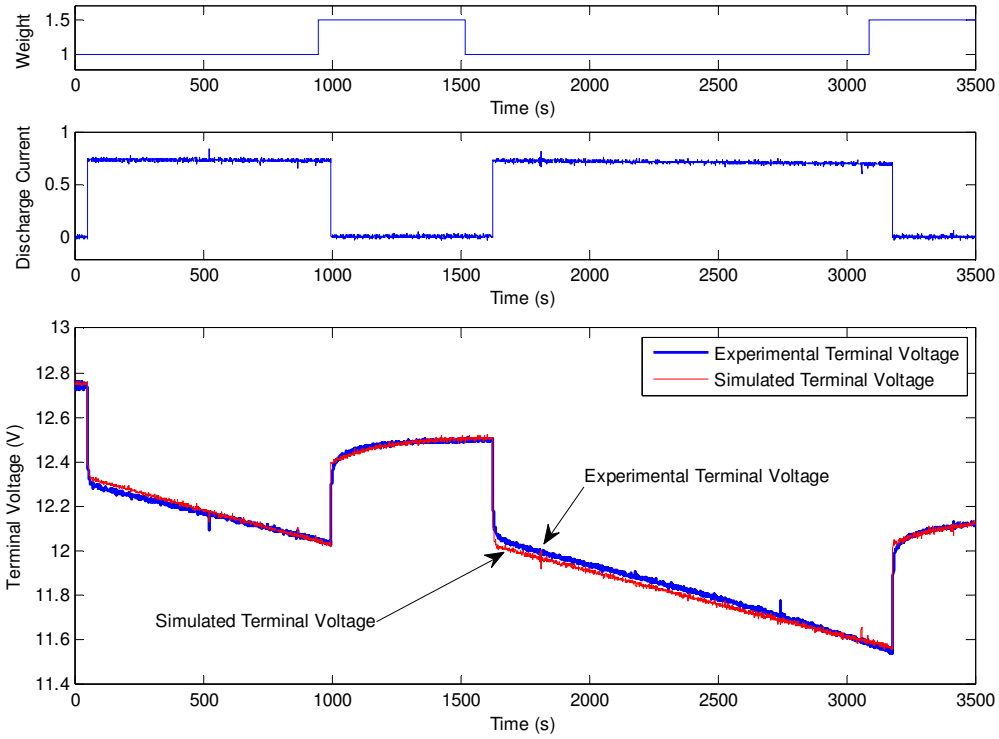

Figure 5-8 Measured and Simulated Result after Parameter Identification

Figure 5-9 shows the mean fitness value and the best in each generation. It can be seen that the best fitness in each generation is decreasing. The mean fitness is unstable because of the mutation operator in the GA that can attempt to find better solutions.

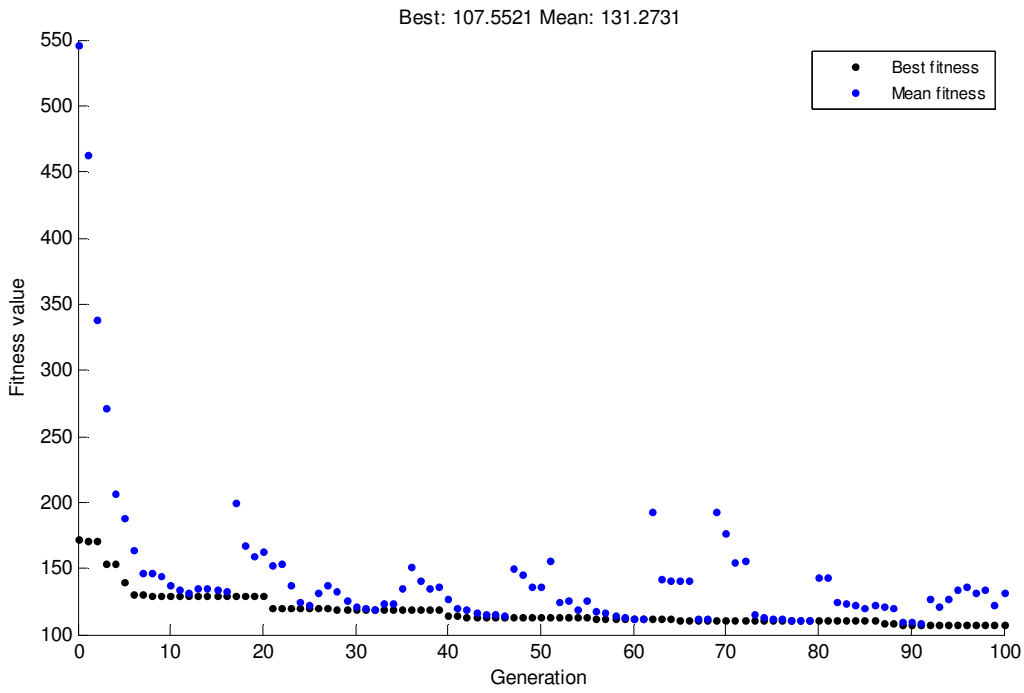

Figure 5-9 Mean and the Best Fitness Values in Each Generation

5.4.3. Battery Model Validation

In order to validate the battery mathematical model, two sets of experimental tests have been adopted to compare with the simulation results.

The inputs of the discharge current and the validation results using two experimental tests are shown in Figure 5-10 and Figure 5-11:

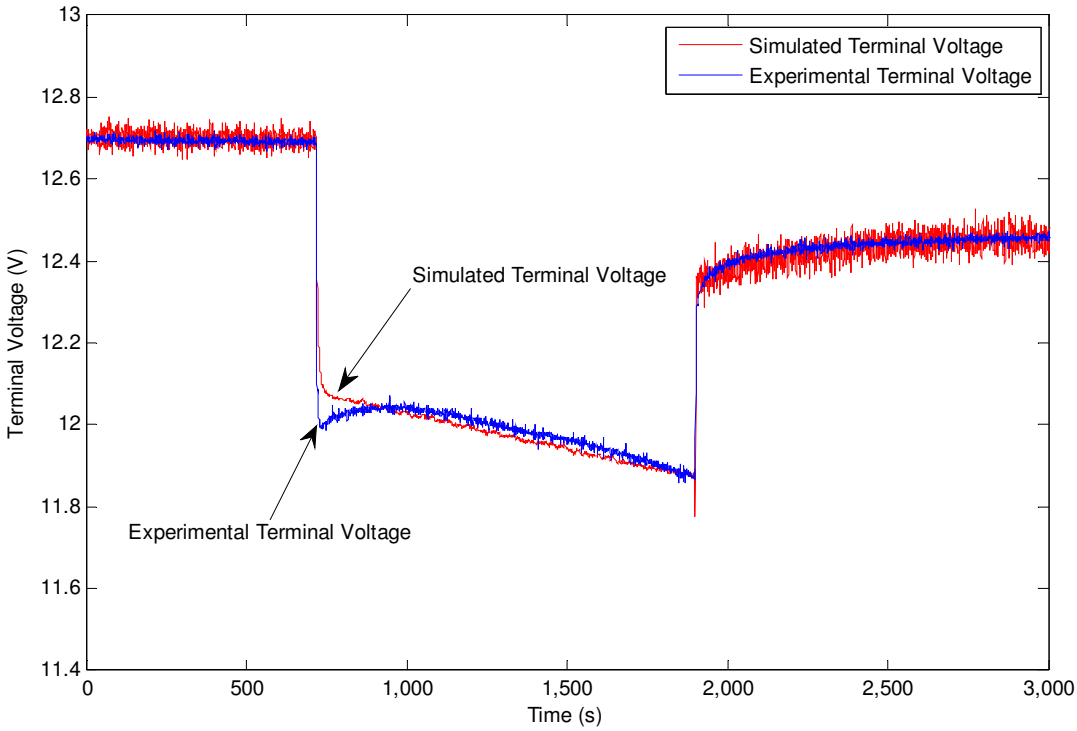

Figure 5-10 Measured and Simulated Terminal Voltage (Validation data 1)

In the simulation that shows in Figure 5-10, the discharge of battery begins at the time of 700s and the simulation result shows a reasonable agreement with the experimental result despite the noise of signal caused by the error of the sensors. It is noticed that, at the beginning of the discharge, there is a difference between the simulated and experimental terminal voltages for about 100 seconds. This difference is studied and so called 'coup de fouet' which often takes place at the beginning of a discharge test when the SOC of battery is high (Perrin, Delaille et al. 2006). However, this 'coup de fouet' behaviour cannot be described in this model. The discharge period lasts for about 1200 seconds and then stops, and after that, the simulation has the similar result with the experiment.

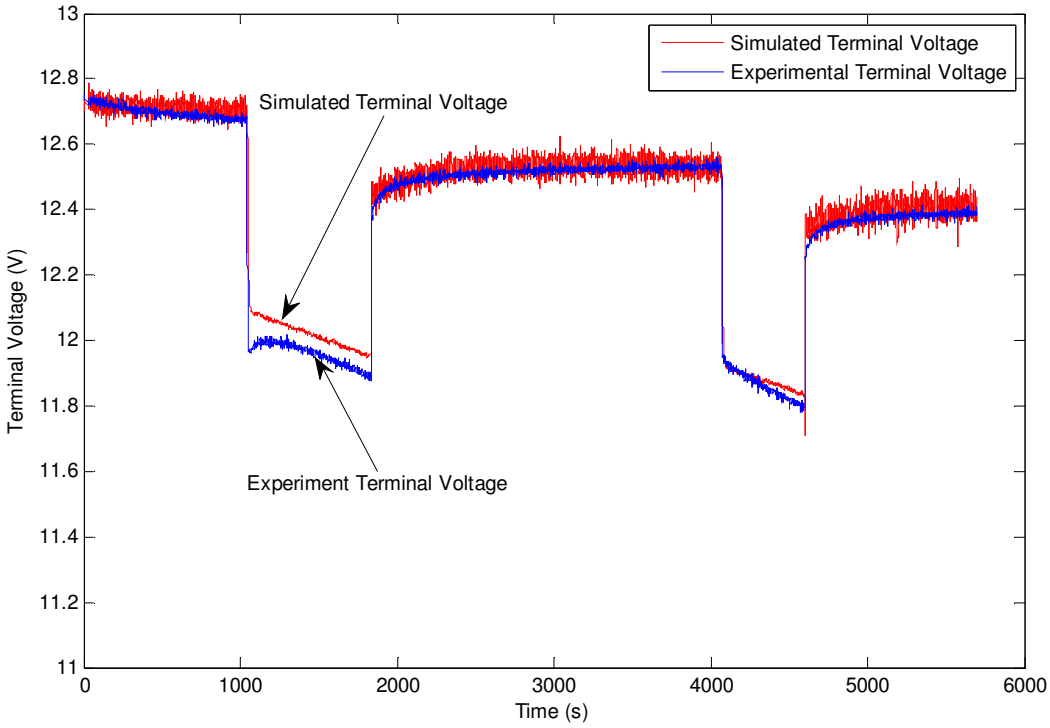

Figure 5-11 Measured and Simulated Terminal Voltage (Validation data 2)

Figure 5-11 shows another group of experimental test to validate the battery model. At the beginning of the experiment, the terminal voltage from the experiment is dropping without any discharge behaviour of battery and that is because of the experiment was carried out when the terminal voltage of lead-acid battery is not steady enough after being charged and that also causes the deviations in the discharge at about 1000-2000 seconds. In this period, the 'coup de fouet' appears again. After the first period, the battery is disconnected from the load until the terminal voltage become steady and the simulation result in this period fits the experiment result well. In the second discharge of this test, it is shown that the 'coup de fouet' does not occur because the SOC is not high. For the similar reason, in the first discharge in this group of the test results, there are

also some deviations in this period. Finally, the simulation result in the last part of figure fits the experimental result is highly satisfied.

The average error of the simulated outputs of the simulation studies and the measured results are studied. Absolute Error and Relative Error is defined as the following equations:

$$AbsError = \frac{1}{N}\sum_{i=1}^{N}\left|V_{sim}(i) - V_{\exp}(i)\right|$$

$$RelError = \frac{1}{N}\sum_{i=1}^{N}\left|\frac{V_{sim}(i) - V_{\exp}(i)}{V_{\exp}(i)}\right|$$

The absolute error and relative error are summarised in Table 5-3.

Table 5-3 AbsError and RelError of Model Validation

	Absolute Error			Relative Error		
	discharging	relaxing	overall	discharging	relaxing	overall
Experimental Test 1 (Identification)	0.0229V	0.0207V	0.0217V	0.1833%	0.1724%	0.1776%
Experimental Test 2 (Validation data 1)	0.0536V	0.0484V	0.0492V	0.4453%	0.3872%	0.4024%
Experimental Test 1 (Validation data 2)	0.0724V	0.0372V	0.0485V	0.6352%	0.3013%	0.5025%

5.5. Summary and Discussions

Identification of the unknown model parameters is discussed in this chapter and a range of possibly suitable methods are reviewed in brief. In this project, Genetic Algorithm is adopted. GAs working principle and its implementation has been

introduced in details in this chapter. The simulation study of two benchmark functions that are commonly used in evaluating evolutionary computation algorithms are employed in order to show the capability of GAs. The parameter identification by tests of a brand new 1.3Ah lead-acid battery is carried out and is validated by two sets of other experimental test results under the same working condition of the same battery.

Chapter 6
The Analysis of State of Health (SOH) in association with the Internal Resistance

6.1. Methodology

As the number of discharge cycles of battery increases in applications, the maximum charges that a battery can offer will decrease. In other words, the SOH battery is deteriorating. But this drop of capacity is not linear and it is also a long progress. At the beginning of the use of battery, the change of capacity is very slow and it is not obvious. After a number of cycles of discharge and charge, this change will get faster and relatively significant.

There are no reliable methods now to calculate the remaining charge capacity, which is the only one determinant of the state of health. The normal method is simply to measure the voltage on its terminals. But this measurement is not accurate on an aged battery. A battery in poor state of health but sufficiently charged can also offer sufficient voltage to appear normal. The only way to determine the capacity accurately is to integrate the discharge current of battery in a full deep discharge, but this method cannot be used too frequently because deep

discharge is harmful for the battery.

In the project, six lead-acid batteries were tested using the test system described in Chapter 4. These batteries were repeatedly discharged and charged for their whole life time so that the information related to different state of health can be revealed as soon as possible. Even though the batteries works frequently, it still takes more than 6 months to make the battery become weak. The testing experiments were carried out and the data was recorded every 2-3 weeks so that important value of state of health is not missed. However, as the change of capacity is a long progress and it is nonlinear, not all the data collected can be used in this project.

Referring the literature (Coleman, Lee *et al*. 2006; Lakhdari and Midoun 2007; Coleman, Hurley *et al*. 2008), an important factor that reflects the change of state of health of a lead-acid battery is the internal resistance. Not only the state of health but also other factors (SOC, DOC, discharge current etc.) can result in variations in internal resistance, a new alternative method that based on the Improved Battery Model in Chapter 4 is adopted in the project.

From the model study in Chapter 4, the internal resistance can be divided into two parts, expressed by $R_0 = R_{00}[1 + A_0(1 - SOC)]$ (Eq 4.7), and $R_1 = -R_{10}\ln(DOC)$ (Eq 4.8). These equations show that the internal resistance is affected by the state of charge (SOC) and depth of charge (DOC) in a discharge cycle. In real applications, batteries are seldom discharged to the full range because a deep discharge could cause some damage to the battery. They are also seldom to be charged to full to prevent the possibility of overcharge that could also bring some

negative effects. Although this issue is not very significant in a valve regulated lead acid battery, it is better to control the working range of depth of charge from 50% to 80% approximately. In this project, the internal resistance of battery in the depth of charge of 65% is studied as a most important factor that related to the state of health. As a little inaccurate of SOC and DOC will induce a comparative big difference in the internal resistance, the method of measuring the internal resistance accurately by an external circuit is discarded.

In Equation 4.7 and Equation 4.8, the author found that there are two other factors that influence the internal resistance besides the SOC and the DOC: R_{00} and R_{10}. Therefore in the project, the values of R_{00} and R_{10} in a specific discharge current are very important to study the internal resistance. The values of these two factors are used in Equation 4.7 and Equation 4.8 to calculate the internal resistance per cell of the battery. The depth of charge is assumed to be 65% for a normal working battery as described previously. In chapter 3, the SOC and the DOC are defined as $SOC = 1 - Q_e / C(0, \theta)$ (Eq. 4.4) and $DOC = 1 - Q_e / C(I_{avg}, \theta)$ (Eq. 4.5). The Capacity is also defined as equation 4.2:

$$C(I, \theta) = \frac{K_c C_{0*} (1 + \frac{\theta}{\theta_f})^{\varepsilon}}{1 + (K_c - 1)(I / I*)^k} \qquad (6.1)$$

in which $K_c = 1.18$, $k = 1.20$ and $I_{avg} = 6 \times I*$ in this project. The relationship between the actual capacity under discharge current I_{avg} and the nominal capacity is:

$$\frac{C(I_{avg},\theta)}{C(0,\theta)} = \frac{\frac{1}{1+(K_c-1)(I_{avg}/I^*)^k}}{\frac{1}{1+(K_c-1)(0/I^*)^k}} = \frac{1}{1+(K_c-1)(I_{avg}/I^*)^k} \approx \frac{1}{2.6} \quad (6.2)$$

Therefore the *SOC* when the *DOC* is 65% is:

$$SOC = 1 - Q_e / C(0,\theta) = 1 - Q_e /(2.6 \cdot C(0,\theta)) \approx 86.5\% \quad (6.3)$$

As described in chapter 5, $A_0 \approx 3$, therefore the internal resistance of an individual cell can be obtained by:

$$r_{cell} = R_0 + R_1 = R_{00}[1 + A_0(1 - SOC)] - R_{10}\ln(DOC) \approx 1.4 \cdot R_{00} + 0.43 \cdot R_{10} \quad (6.4)$$

and for a six-cell lead-acid battery, the internal resistance:

$$r_{battery} = r_{cell} \times 6 = 8.4 \cdot R_{00} + 2.58 \cdot R_{10} \quad (6.5)$$

6.2. The identification of C_0, R_{00} and R_{10}

In the eight parameters identified previously in Chapter 5, there are only three parameters can be affected by the change of battery conditions. Therefore the other five parameters ($E_{m0}, K_E, A_0, \tau_1, \tau_2$) can be treated as a constant for a battery. The parameters that related to the battery condition, R_{10}, R_{00} and C_{0^*}, are the key problems which the project focused on. C_{0^*} represents the state of health, while the R_{10}, R_{00} stands for the internal resistance parameters. Here again, the Genetic algorithm is adopted to identify these three parameters.

In this project, the battery have been discharged and charged in hundreds of cycles to simulate the capacity loss in the normal applications, which is described by the

state of health in this project. In order to find out the different behaviour of internal resistance in different state of health, experimental tests have been carried out in different state of health of the battery.

The first test is carried out when the battery is brand new, and the data is also used to identify the other parameters of the battery model as described in the previous chapter. The second group of data is collected after 300 discharge cycles approximately, and the third test took place after 200 more cycles. The number of discharge cycles between the last four tests is only about 50 because the change of State of Health is more significant. The identified parameters of a battery in different state of health are shown in table 6-1.

Table 6-1 Battery Remaining Capacity and Internal Resistance

	Remaining Capacity C_{0*} (Amp·s)	SOH	R_{00}	R_{10}	RelError	Internal Resistance (Ohm)
Test 1	4819.8	100%	0.0609	0.0220	0.1756%	0.5683
Test 2	4486.1	93.14%	0.0654	0.0103	0.7428%	0.5759
Test 3	3802.5	78.89%	0.0635	0.0191	0.2812%	0.5827
Test 4	3383.0	70.19%	0.0573	0.0509	0.7265%	0.6126
Test 5	3062.5	63.54%	0.0604	0.0582	0.4340%	0.6575
Test 6	2607.2	53.06%	0.0703	0.0368	0.1342%	0.6855

And the terminal voltages simulated and measured are shown as the following figures. The same as previous figures, the blue lines represent the measured outputs while the red lines represent the simulation results.

The test shows in figure 6-1 the same as the test which is used to describe the genetic algorithms and the battery parameter identification in chapter 5. Detailed

description and analysis are given in chapter 5.

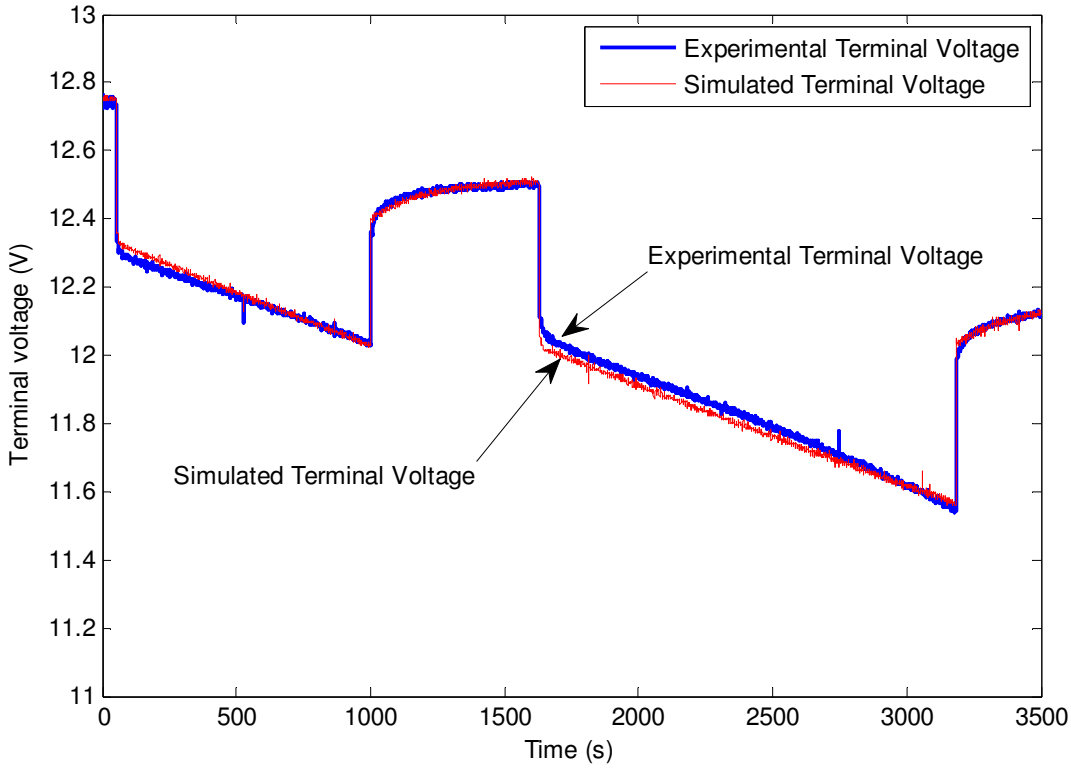

Figure 6-1 Experimental and Simulated Terminal Voltage of Test 1 (SOH = 100%)

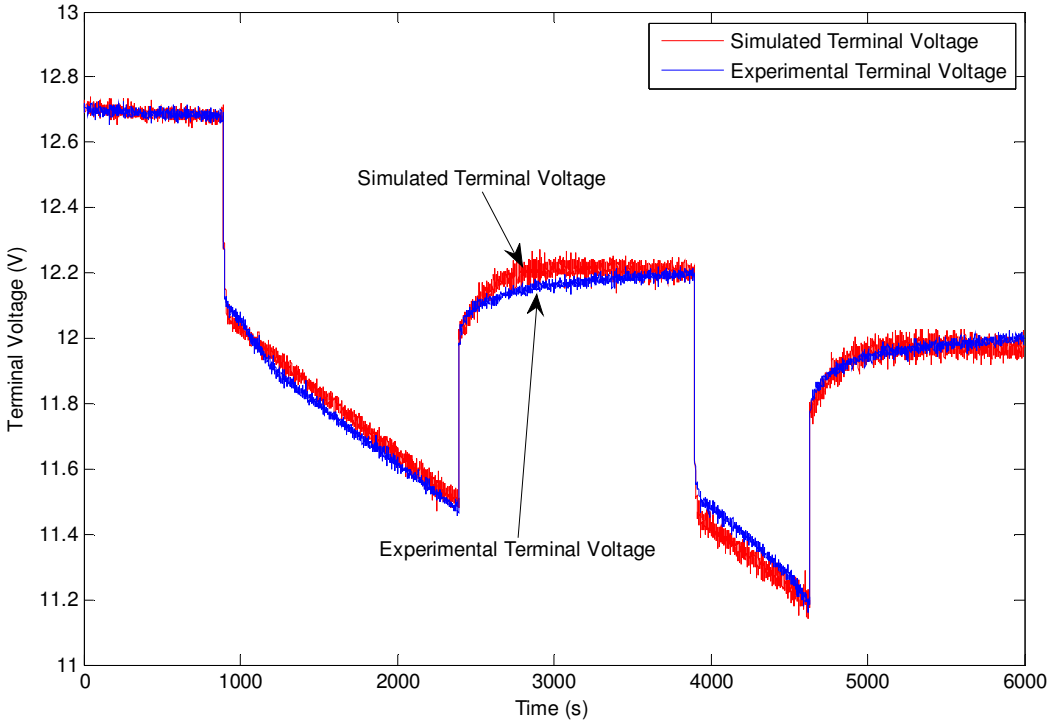

Figure 6-2 Experimental and Simulated Terminal Voltage of Test2 (SOH= 93.14%)

The experiment shown in figure 6-2 is tested several months after the first experimental test. In the period that the first discharge begins, the experimental result shows a different slope in terminal voltage. The reason is probably that the battery have just charged to full by a charger and it's the capacitor had not fully discharged. After that when the discharge stopped, there is a deviation in the simulation voltage. In the author's opinion, that is because of the accuracy of R_{10} and R_{00}. If the value of R_{10} is greater and that of R_{00} is smaller, the simulation result should fit the experimental result. In the second discharge period of the discharge test, there is also a little difference in the experimental and simulation result caused by the inaccuracy of battery parameters. But it shows a good agreement when the discharge stopped.

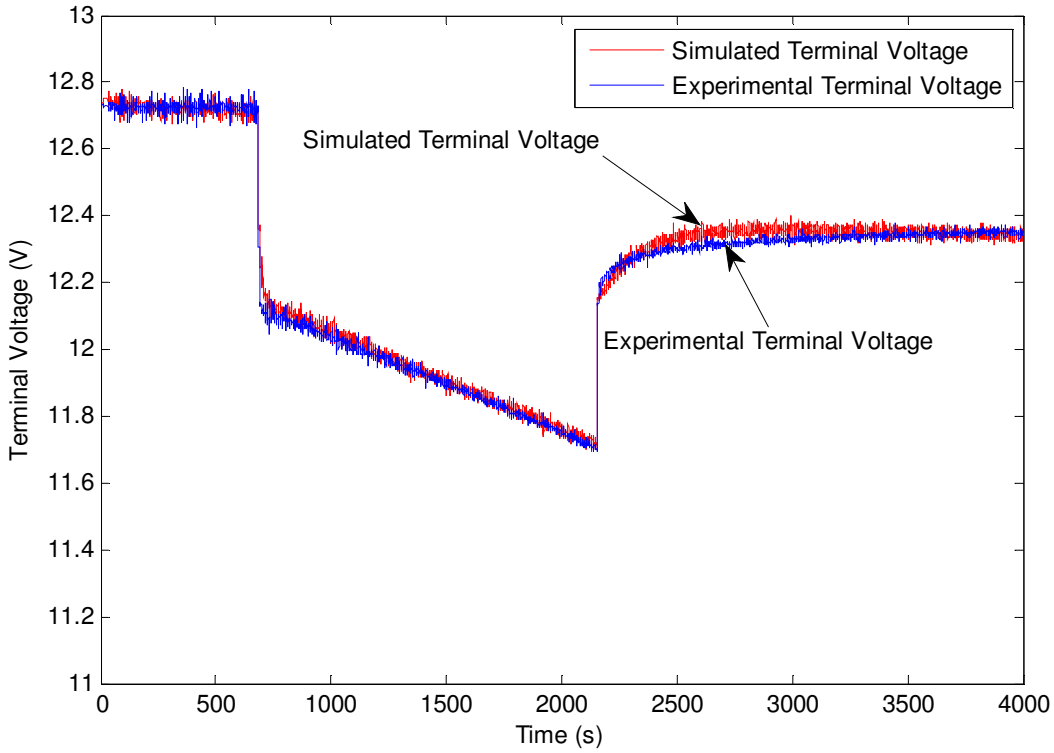

Figure 6-3 Experimental and Simulated Terminal Voltage of Test3 (SOH= 78.89%)

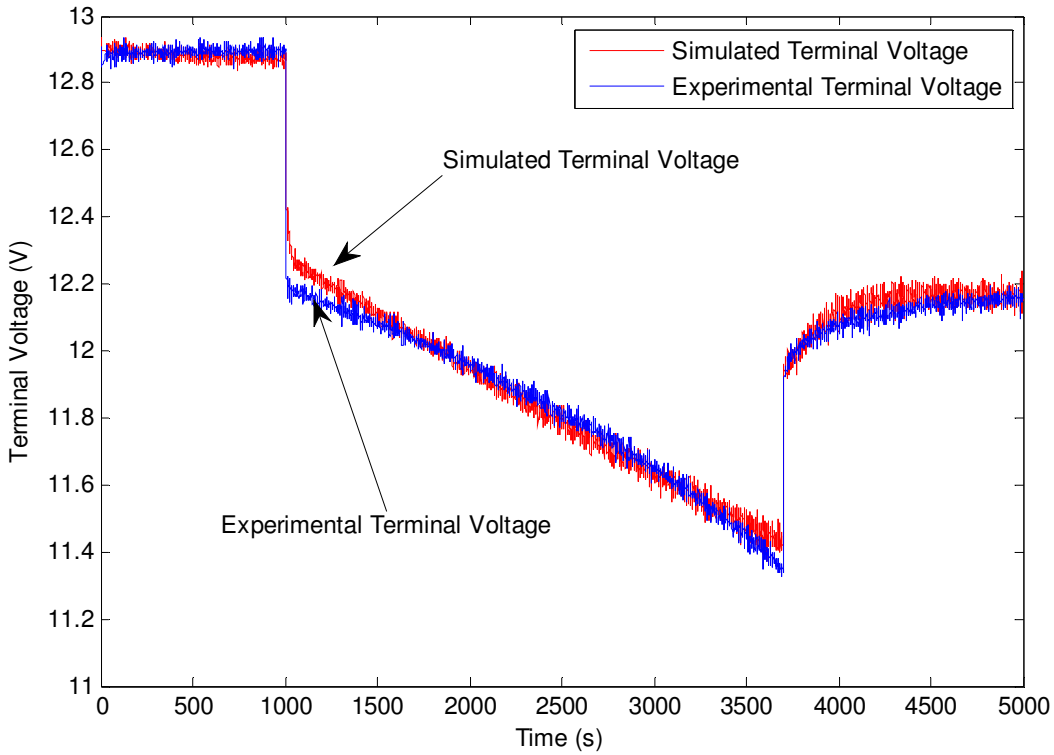

Figure 6-4 Experimental and Simulated Terminal Voltage of Test4 (SOH= 70.19%)

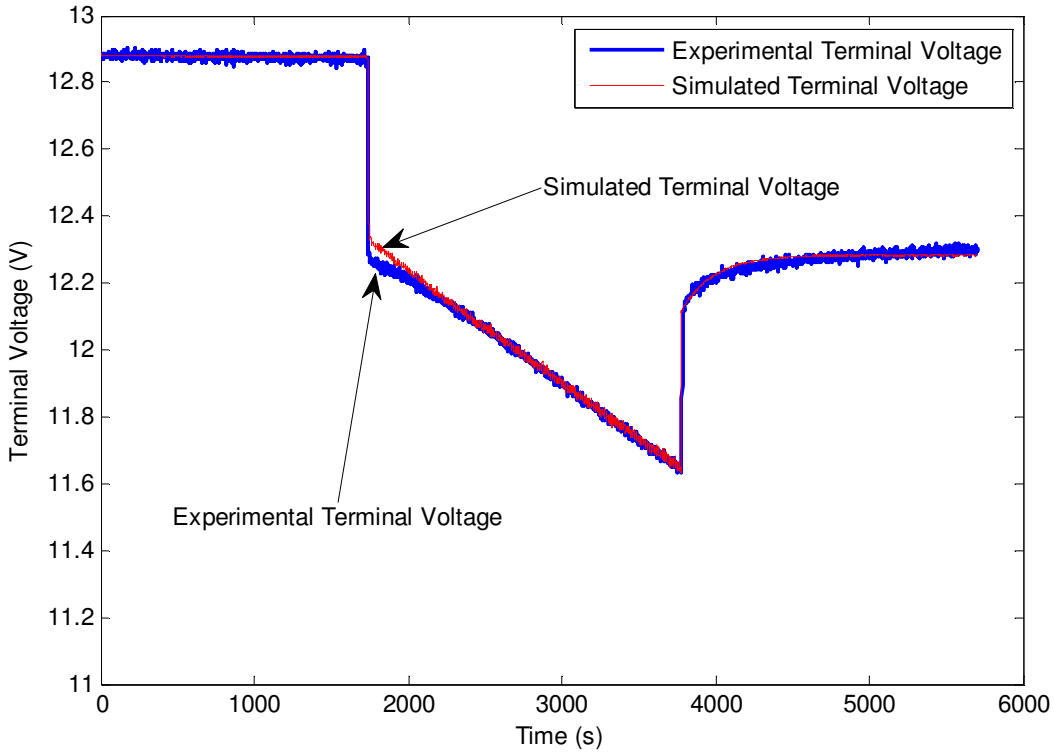

Figure 6-5 Experimental and Simulated Terminal Voltage of Test5 (SOH= 63.54%)

Figure 6-3, figure 6-4 and figure 6-5 show the test results of the battery when the SOH drops to its 80%, 70% and 60%. It is shown that the simulation result in figure 6-3 fits the experimental result until the end of test when the discharge of battery has just stopped. The inaccuracy of the R_{10} and R_{00} is also the main cause of the deviation. The overall simulation result in figure 6-4 figure 6-5 are good to express the battery behaviour.

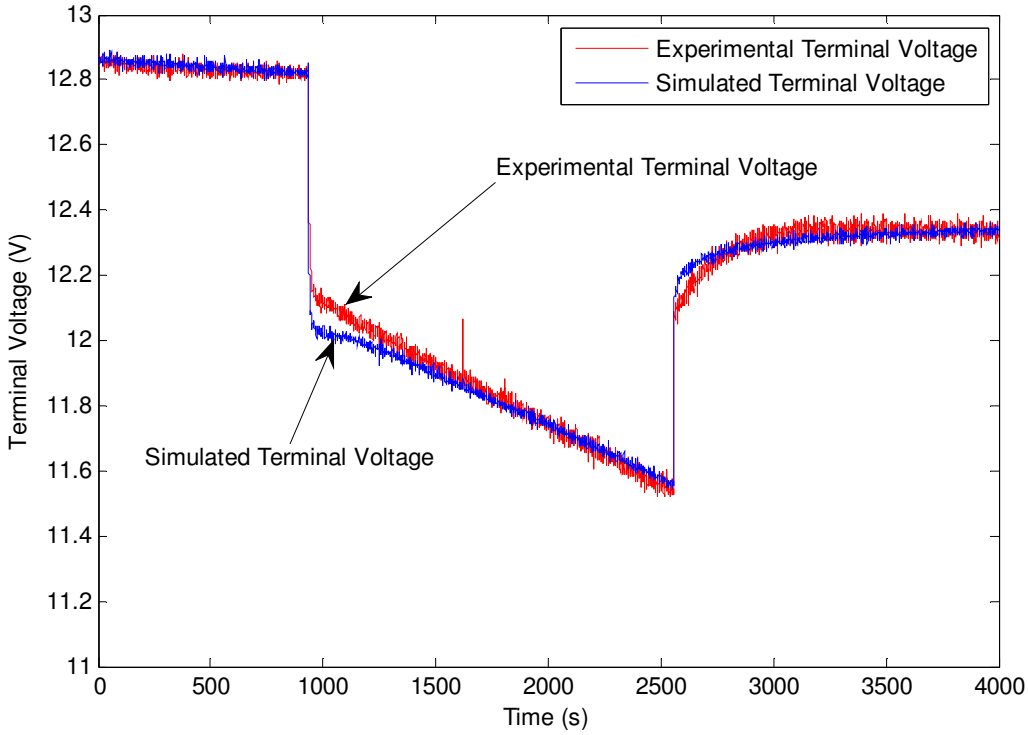

Figure 6-6 Experimental and Simulated Terminal Voltage of Test6 (SOH= 53.06%)

In the parameter identification of test shown in figure 6-6, the remaining capacity is only about 1/2 of the initial capacity when the battery is brand new. During the discharge period, the simulation and experimental result is not fitting very well and the slopes of them are not the same. This is probably also caused by insufficient idle time after being charged and the capacitor had not fully discharged.

Figure 6-7 represents the internal resistance value in different state of health as described in table 6-1.

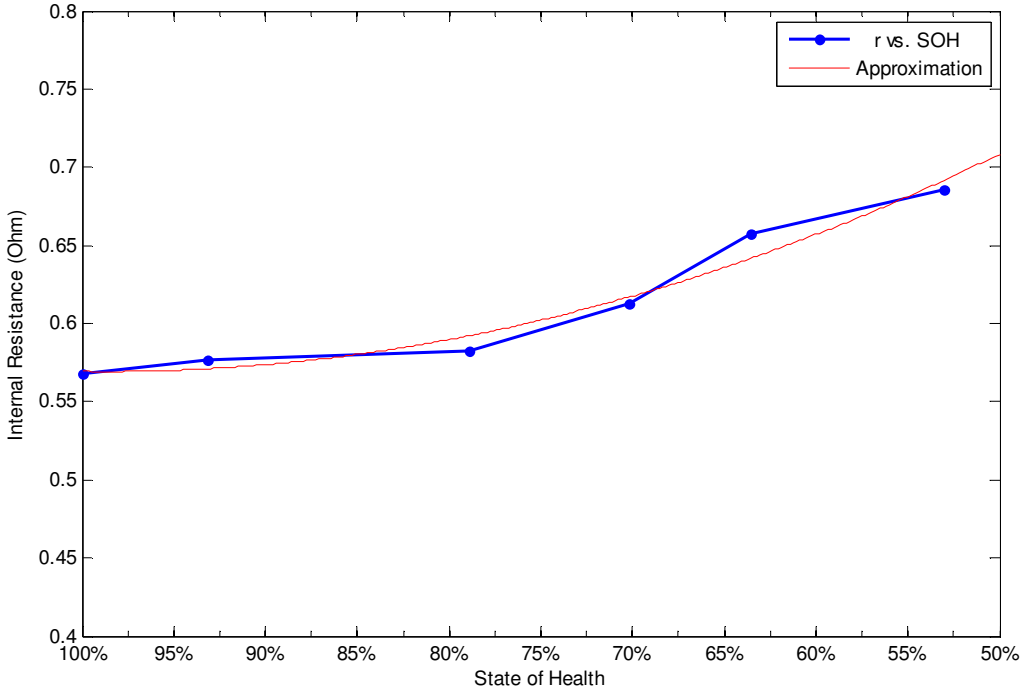

Figure 6-7 Change of Internal Resistance in Different State of Health (Battery 1)

It is shown that the internal resistance is increasing when the state of health of a lead-acid battery decreases. This progress is at first very slow when the battery is new. But after a number of discharge cycles, the remaining capacity of battery drops to about 75% of the initial capacity when the battery is new, and the increase of internal resistance become faster. When the state of health is brought down to about 50%, which means that the battery cannot offer enough energy as new, the value of internal resistance is increased by 30% approximately. At present there is not a published quantitative description of the internal resistance when the capacity changes yet but it has been agreed that the internal resistance increases while the battery health deteriorates.

Similar tests have been carried out on 5 other batteries with the same nominal

capacity and the changes of their internal resistances are given as figure 6-8. It is not possible to deduce a statistical approximation equation only based on the existing data, but it can be seen from the figure that the performance of internal resistance under different state of health shows an agreement in a certain extent.

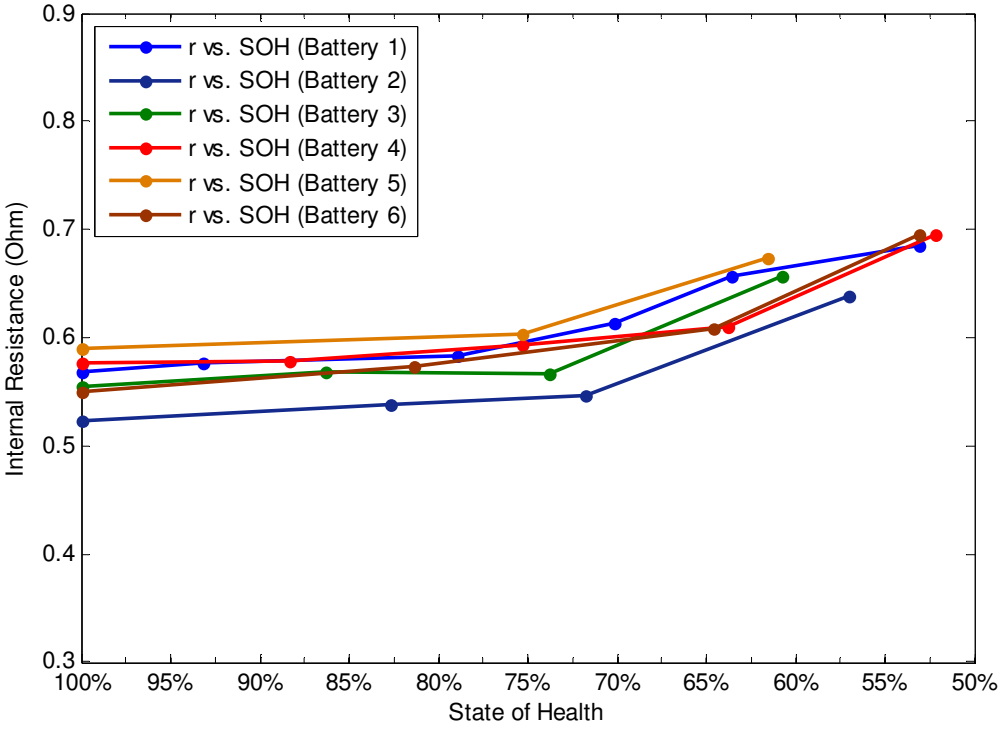

Figure 6-8 Change of Internal Resistance in all 6 Batteries

6.3. Summary and Discussions

The determination of battery remaining capacity accurately is becoming increasingly important in modern battery managements. This currently is mostly obtained by integrating the discharge current of a full discharge, but this progress usually causes a negative effect on most of the batteries. There is also a view that

the state of health, which represents the percentage of remaining capacity of a weak battery compared with the initial capacity when brand new, can affect the internal resistance therefore the battery state of health can be obtained by the study of battery internal resistance. However, from the analysis based on the mathematical model and the experimental results, it can be concluded that other parameters can also cause variations of the internal resistance, which make the estimation of the state of health more challenging.

This chapter describes a new alternative method that based on the Improved Battery Model and the key parameters of the model. The remaining maximum capacity of a used battery, which represents the SOH of the battery, is related in the internal resistance under the depth of charge of 65%, which is expressed by the parameters of R_{00} and R_{10}. These parameters can be identified by genetic algorithms. A result that quantifies the change of internal resistance in different SOH values has been concluded based on the analysis of a series of experimental tests.

Chapter 7
Conclusions and Future Research

This chapter summarizes the major achievements of the presented research work in the field of battery modelling and state of health analysis. Possible direction of further research work is also described briefly in this chapter.

7.1. Summary

Lead-acid batteries are used in various industrial sectors and are irreplaceable due to their low price. In areas where lead-acid batteries are employed as an energy storage device, the capacity loss caused by the repeated discharge/charge cycles is very common. This drop of capacity can neither be avoided nor be repaired by using current technologies. As a result it is essential to know whether the battery is able to meet the demand and if it should be replaced on time.

In this thesis, a study on the capacity status of a battery and its relation to the internal resistance had been conducted and this thesis established a novel model based method to quantify the battery health. An Equivalent Circuit Mathematical model for the discharging progress of a lead-acid battery has been developed for this purpose and is implemented under Matlab/SIMULINK software environment.

The model involves most of the important concepts of a battery to reflect the dynamic response of terminal voltage when discharging.

A series of experimental tests have been carried out during the project for the model validation and the study of the state of health. Six 12V-1.3Ah lead-acid batteries with the same rated capacity are discharged and recharged from brand new to obtain different values of state of health. Genetic algorithm has been employed to identify the unknown parameters of the battery model in each state of health, and the identified parameters are used as the factors that reflecting the state of health and the internal resistance. The internal resistances corresponding different state of health have been collected and recorded. A result was found in the thesis that for the 12V-1.3Ah lead-acid battery, which is used in the experimental tests, the value of internal resistance is increased by 25% approximately if the SOH of battery drops to 50%.

7.2. Limitations

The key limitation of the method introduced in this thesis is that it is based on the parameter identifications of the model, which means a test is still needed in order to obtain the state of health. The major reason is that the mathematical model does not include the charging progress of battery, which is also an important period of the battery duty cycle. Another limitation is that all the tests of the state of health estimation are carried out at the same discharge rate because of the variation of the internal resistance in different discharge rate as discussed in chapter 4. Finally,

The ‘coup de fouet’ behaviour that of took place at the beginning of discharge when batteries are full is not able to be simulated in the current version of mathematical model.

7.3. Future Research Work

Following the limitations of the project, some future research can be carried out in three steps based on the model improvements and the practical applications of the algorithm.

First of all, improvements of the discharging battery model can be carried out, which can mainly focus on the study of the battery internal resistance in different discharge rates. Equations of internal resistances that can withstand the change of discharge rate will make the model capable for online applications. Studies on the relationship between the electromotive force and the state of charge can also lead to a solution of the ‘coup de fouet’ behaviour and a better simulation result.

Another research work on the model modification is that the behaviour of battery to the mathematical model when a battery is being charged can be involved by which the monitoring system of battery can be implemented in the whole duty cycles. This part of work can be focused on the parasitic branch in the mathematical model described in chapter 3.

Further work should also reveal the variations of state of health in different duty

cycles and an algorithm based on this change should be designed to estimate the remaining life-time of a lead-acid battery. The value of current state of health and the estimated raining life-time should also be considered as major outputs in this period of work. It is also possible to design an online management device of battery to estimate the life-time and the state of health.

References

Anon. (2006). "Global Wind Energy Council (GWEC) statistics [online]." from http://www.gwec.net/uploads/media/07-02_PR_Global_Statistics_2006.pdf.

Anon. (2007). "Battery Types: Flooded versus AGM and Gel [online]." Retrieved February 13,, 2007, from http://www.vonwentzel.net/Battery/01.Type/.

Anon. (2007). "BP Statistical Review of World Energy June 2007 [online]." from http://www.bp.com/liveassets/bp_internet/globalbp/globalbp_uk_english/reports_and_publications/statistical_energy_review_2007/STAGING/local_assets/downloads/spreadsheets/statistical_review_full_report_workbook_2007.xls.

Anon. (2007). "International Energy Outlook 2007 [online]." from http://www.eia.doe.gov/oiaf/ieo/highlights.html.

Ball, R. J., Evans, R., and Stevens, R.. (2002). "Finite element (FE) modelling of current density on the valve regulated lead/acid battery positive grid." **Journal of Power Sources 103**(2): 213-222.

Bernardes, A. M., Espinosa, D. C. R., and Tenório J. A. S. (2004). "Recycling of batteries: a review of current processes and technologies." **Journal of Power Sources 130**(1-2): 291-298.

Berndt, D. (1993). **Maintenance-Free Batteries -- A Handbook of Battery Technology**. Somerset: Research Studies Press Ltd.

Berndt, D. (2001). "Valve-regulated lead-acid batteries." **Journal of Power Sources 100**(1-2): 29-46.

Berndt, D. (2009). Electrochemical Energy Storage. **Battery Technology Handbook**, CRC Press.

Casacca, M. A. and Salameh, Z. M. (1992). "Determination of lead-acid battery capacity via mathematical modeling techniques." **Energy Conversion, IEEE Transaction on 7**(3): 442-446.

Ceraolo, M. (2000). "New dynamical models of lead-acid batteries." **Ieee Transactions on Power Systems 15**(4): 1184-1190.

Chan, H. L. and Sutanto D. (2000). A new battery model for use with Battery Energy Storage Systems and Electric Vehicles Power Systems. **2000 Ieee Power Engineering Society Winter Meeting - Vols 1-4, Conference Proceedings:** 470-475.

Chen, M. and Rinc´on-Mora G.. A. (2006). "Accurate electrical battery model capable of predicting runtime and I-V performance." **IEEE TRANSACTIONS ON ENERGY CONVERSION, VOL. 21,**(NO. 2,): 504-511.

Chipperfield, A. J., Fleming P. J., and Fonseca C. M. (1994A). Genetic algorithm tools for control systems engineering. **Adaptive computing in engineering design and control**. Plymouth, UK.

Chipperfield, A. J., Fleming P. J., Pohlherim, H and Fonseca C. M. (1994B). Genetic algorithm toolbox for use with Matlab**:** Department of automatic control and systems engineering, University of Sheffield

Crompton, T. R. (2000). **Battery Reference Book**, Third Edition, Oxford: Elsevier Newnes.

Cun, J. P., Fiorina, J. N., Fraisse, M., Mabboux, H. A. and Mabboux H. "The

experience of a UPS company in advanced battery monitoring." **Telecommunications Energy Conference, 1996. INTELEC '96., 18th International:** 646 - 653**.**

Durr, M., Cruden, A., Gair, S. and McDonald, J. R. (2006). "Dynamic model of a lead acid battery for use in a domestic fuel cell system." **Journal of Power Sources 161**(2): 1400-1411.

Esfahanian, V., Torabi F. and Mosahebi (2008). "An innovative computational algorithm for simulation of lead-acid batteries." **Journal of Power Sources 176**(1): 373-380.

Gillioli, R. and Cerolo P. (1990). Charge and discharge fourth order dynamic model of the lead battery. **10th int'l Electric Vehicle Symposium**. Hong Kong. **p.1-9**.

Glendenning, I. (1981). "Compressed air storage." **Physics in Technology 12**(3): 103-10.

GONG, Q. (2005). "Modeling study of a vehicle traction battery model ". **CHINESE LABAT MAN 2005**, Vol 42; Numb 2; issu 155, pages 76-79

Houck, C., Joines J. and Kay, M. (1995). A Genetic Algorithm for Function Optimization: A Matlab Implementation. NCSU-IE. **TR 95-09**.

Jacobi, W. (2009). Lithium Batteries. **Battery Technology Handbook**, CRC Press.

Jayne, M. G. and Morgan C. (1986). a new mathematical model of lead acid battery for electric vehicles. **Eighth Int'l electric vehicle conference**. Washington D.C.

Juvonen, M. (2003). "Large-Scale Energy Storage Systems [online]." from http://www.doc.ic.ac.uk/~matti/ise2grp/energystorage_report/storage.html.

Lee, J. H., Lee, K. Y. and Lee, J. Y. (1996). "Self-discharge behaviour of sealed Ni-MH batteries using MmNi3.3+xCo0.7Al1.0-x anodes." **Journal of Alloys and Compounds 232**(1-2): 197-203.

Liaw, B. Y., Gu W. B. and Wang, C. Y. (1997). Numerical simulation of coupled electrochemical and transport processes in battery systems, **Proceedings of the Intersociety Energy Conversion Engineering Conference,** Honolulu, HI, USA, IEEE.

Lu, S., Meegahawatte D. H., Guo, S., Hillmansen, S., Roberts, C. and Goodman, C. J. (2008). Analysis of energy storage devices in hybrid railway vehicles. **Railway Engineering - Challenges for Railway Transportation in Information Age, 2008. ICRE 2008**. International Conference on.

Mantell, C. L. (1984). **Batteries and energy systems**. Second Edition, McGraw-Hill Inc.

MathWorks Inc. (2004). Genetic Algorithm Direct Search Toolbox V1.02, MathWorks,Inc.

MPowerSolutionsLtd. (n.d.). "Alternative Energy Storage Methods [online]." from http://www.mpoweruk.com/.

Okoshi, T., Yamada K., Hirasawa, T. and Emori, A. (2006). "Battery condition monitoring (BCM) technologies about lead-acid batteries." **Journal of Power Sources 158**(2): 874-878.

Perrin, M., Delaille A. Huet, F. and Hernout, L. (2006). "Study of the "coup de fouet" of lead-acid cells as a function of their state-of-charge and state-of-health." **Journal of Power Sources 158**(2): 1019-28.

Pham, D. T. and Karaboga D. (1998). **Intelligent Optimisation Techniques:**

Genetic Algorithms, Tabu Search, Simulated Annealing and Neural Networks, New York: Springer-Verlag New York, Inc.

RailPower Hybrid Technologies , C. (n.d.). "Benifits of Hybrid Locomotives [online]." from http://www.railpower.com/products_hl_benefits.html.

Rand, D. A. J., Moseley P. T. and Garche, J. (2004). **Valve-Regulated Lead-Acid Batteries**, Elsevier.

Ruetschi, P. (2004). Aging mechanisms and service life of lead-acid batteries, **Journal of Power Sources 127** (1-2): 33-44 Switzerland, Elsevier.

Salameh, Z. M., Casacca M. A. and Lynch, W. A. (1992). "A mathematical model for lead-acid batteries." **IEEE Trans. on Energy conversion Vol.7 No. 1**.

Sato, Y., Takeuchi, S. and Kobayakawa, K. (2001). "Cause of the memory effect observed in alkaline secondary batteries using nickel electrode." **Journal of Power Sources 93**(1-2): 20-24.

Sims, R. I., Carnes, J. C., Dzieciuch, M. A. and Fenton, J. E. (1990). Computer modeling of Automotive lead acid batteries, Ford Research Laboratories Technical Report.

Smil, V. (2007). **Energy at the Crossroads**. Massachusetts, Achorn Graphic Services, Inc.

Ter-Gazarian, A. (1994). **Energy storage for power systems**. London, Peter Peregrinus Ltd.

TNI_Ltd. (2007). "Battery history [online]." from http://www.europulse.com/battery_history/battery_history.htm.

Tuck, C. D. S. (1991). **Modern Battery Technology**. Ellis Horwood Ltd

Wei, J. (2007). Development of Coal Mill and Aggregate Load Area Models in

Power Systems using Genetic Algorithms, University of Liverpool. **PhD**.

Wikipedia. (n.d.). "Lead-Acid Battery [online]." from http://en.wikipedia.org/wiki/Lead-acid.

Wikipedia. (n.d.). "Rechargeable Batteries [online]." from http://en.wikipedia.org/wiki/Rechargeable_battery.

Wikipedia. (n.d.). "VRLA [online]." from http://en.wikipedia.org/wiki/VRLA.

Zhang, Y. L., Liu, P. H., Zhang, Q. Y. and Cheng, W. (2010). "Separation of cadmium(ii) from spent nickel/cadmium battery by emulsion liquid membrane." **Canadian Journal of Chemical Engineering 88**(1): 95-100.

Appendix I: SIMULINK Diagrams of Battery Model

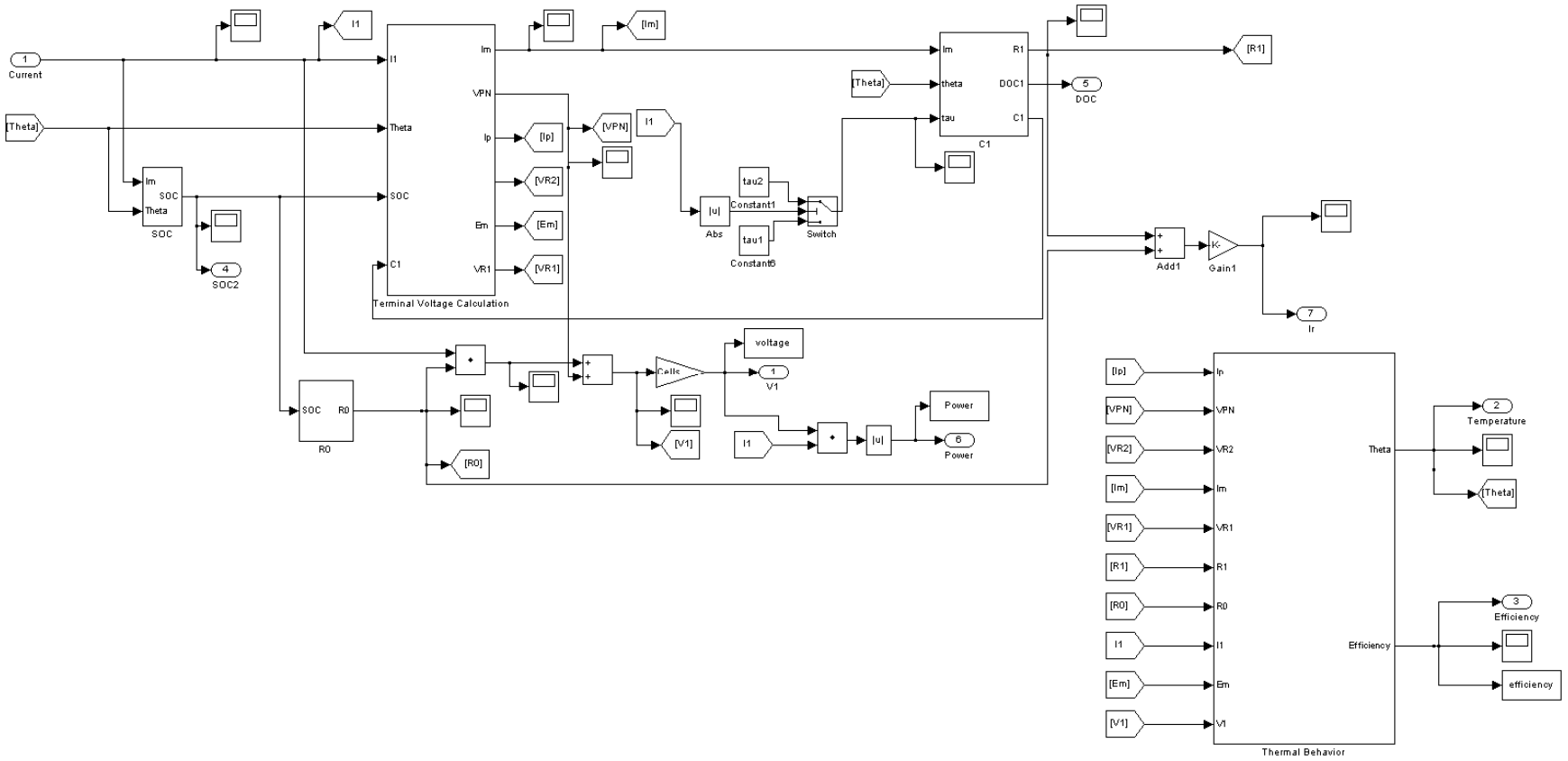

Figure A-1 SIMULINK Diagrams of "Main Block"

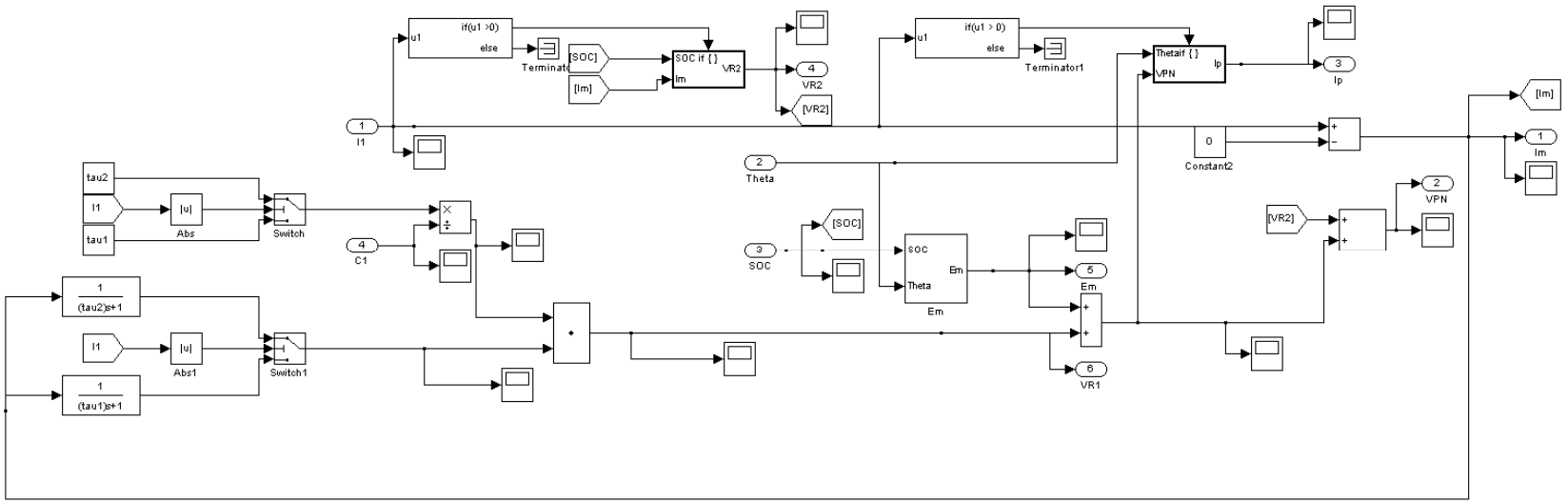

Figure A-2 SIMULINK Diagrams of “Terminal Voltage Calculation”

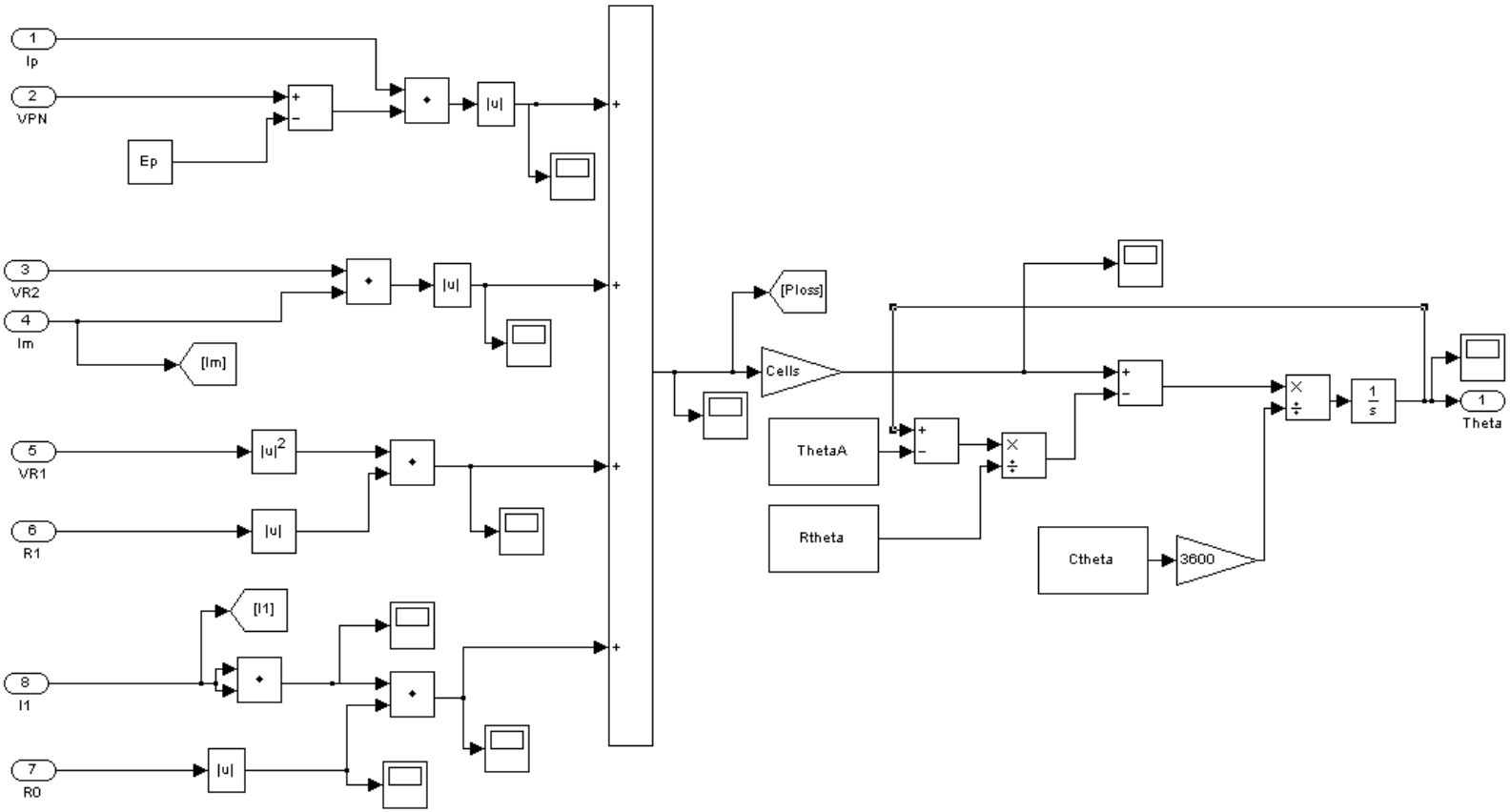

Figure A-3 SIMULINK Diagrams of “Thermal Behaviour”

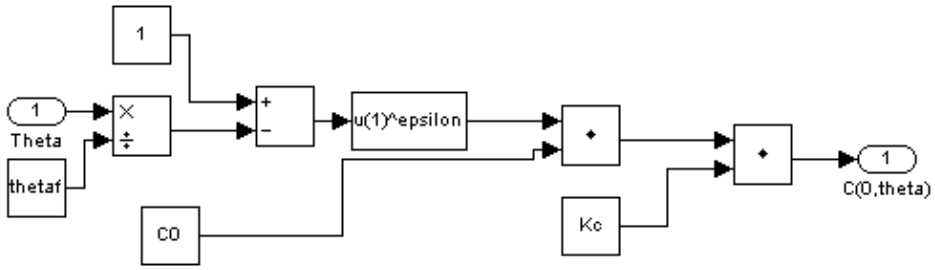

Figure A-4 SIMULINK Diagrams of “Battery Capacity”

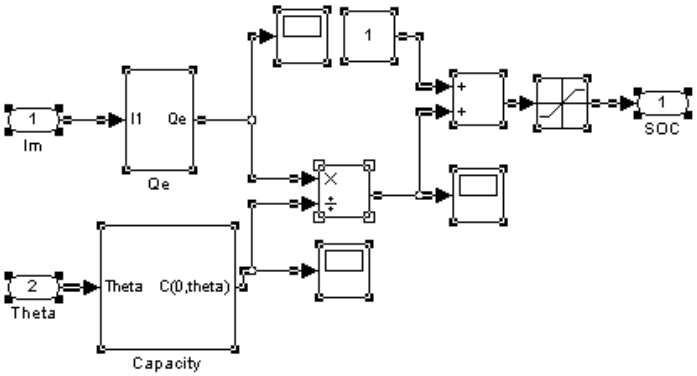

Figure A-5 SIMULINK Diagrams of “Battery State of Charge”

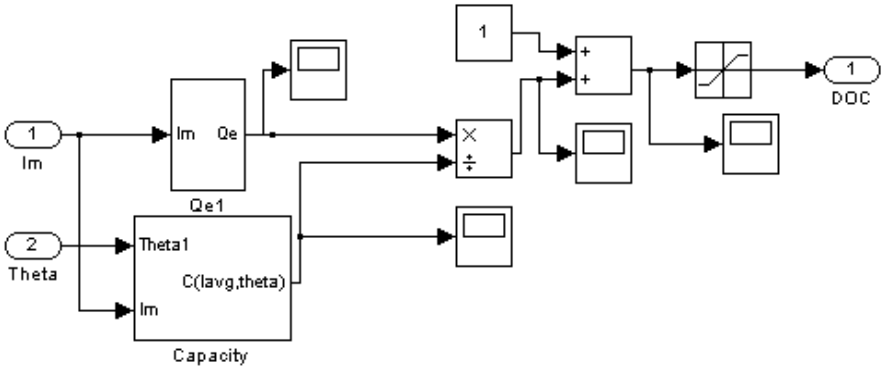

Figure A-6 SIMULINK Diagrams of “Battery Depth of Charge”

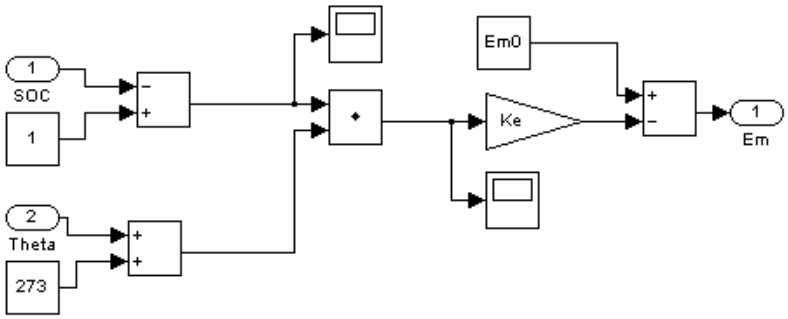

Figure A-7 SIMULINK Diagrams of “Battery Electromotive Force”

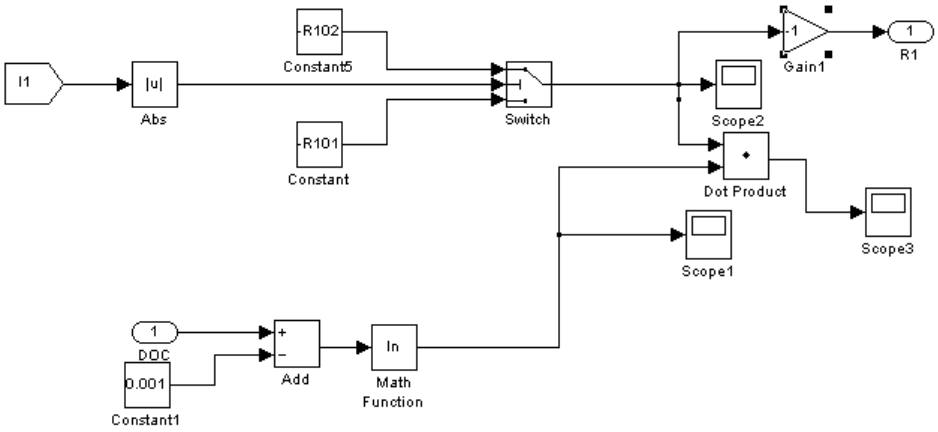

(a)

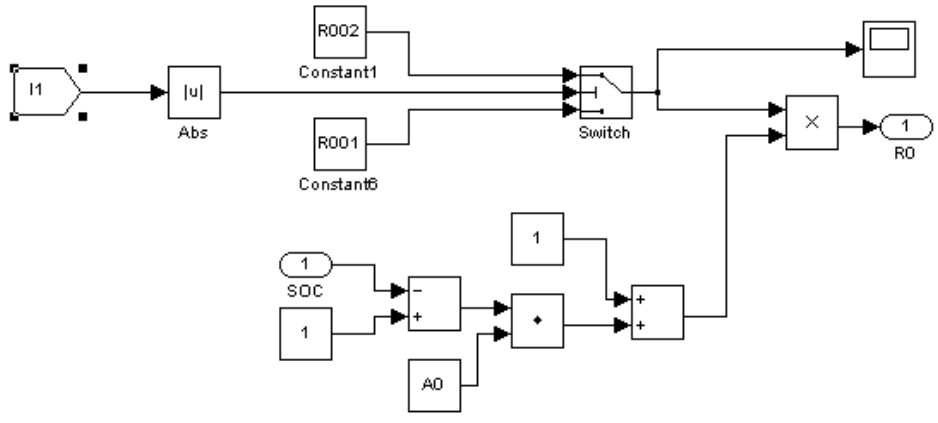

(b)

Figure A-8 SIMULINK Diagrams of “Battery Internal Resistance”

Appendix II:

List of Publications

S. Hillmansen, S. Lu, D. H. Meegahawatte, S. Guo, C. Roberts, and C. J. Goodman, Analysis of Energy Storage Devices in Hybrid Railway Vehicles, International Conference on Railway Engineering 2008, p68-73, Hong Kong, China, 25-28 March, 2008

Y Yin, X Luo, S Guo, Z Zhou, J Wang, A battery charging control strategy for renewable energy generation systems, The Proceedings of World Congress on Engineering 2008, Vol 1, pp356-361, London, UK, 2-4 July, 2008

S. Guo, S. Hillmansen, Y. Yin, J. Wang, State of Health Monitoring of Lead-acid Batteries, Proceedings of the 14th International Conference on Automation & Computing, pp250-254, Brunel University, West London, UK, 6 September 2008

Y. Yin, C. Li, Z. Zhou, Q. Liu, S. Guo, X. Luo, J. Wang, Design and Realization of a PS/2 Keyboard Interface in Embedded system, Proceedings of the 14th International Conference on Automation & Computing, pp160-163, Brunel University, West London, UK, 6 September 2008

Yin, Y., Wang, J., Luo, X., Guo, S., Development of a battery charging management unit for renewable power generation, a book chapter in *Advances in Electrical Engineering and Computational Science*, Edited by Sio-Long Ao and Len Gelman, pp33-46, Springer, 2009.

Wang, J., Wei, J.L., Guo, S., Condition monitoring of power plant milling process using intelligent optimization and model based techniques, accepted as a chapter in the book of *Fault Detection* in March 2009.

S. Guo, S. Hillmansen, J. Wang, Model Based Analysis of Battery State of Health using Genetic Algorithms, accepted by the International Conference on Systems Engineering (ICSE), Coventry, 8-10 September 2009